GeoScienceWorld
Lithosphere
Volume 2023, Article ID lithosphere_2023_192, 20 pages
https://doi.org/10.2113/2023/lithosphere_2023_192

Lithosphere

*Research Article*

# Volcanic Age and Geochemistry of the Permian Linxi Formation in Northeast China: Implications for the Tectonic Evolution of the Paleo-Asian Ocean

**Haihua Zhang**,[1,2] **Hua Zhang**,[3] **Shuzhong Shen**,[4] **Zifu Zhao**,[1] **Liang Qiu**,[5] **Shuwang Chen**,[2] **Jian Zhang**,[2] **Fanhao Gong**,[2] **Yongfei Li**,[2] **Yuejuan Zheng**,[2] **Shouliang Sun**,[2] **and Yujin Zhang**[2]

[1]*CAS Key Laboratory of Crust-Mantle Materials and Environments, School of Earth and Space Sciences, University of Science and Technology of China, Hefei 230026, China*
[2]*Shenyang Center of China Geological Survey, Shenyang 110034, China*
[3]*State Key Laboratory of Palaeobiology and Stratigraphy, Nanjing Institute of Geology and Palaeontology and Center for Excellence in Life and Paleoenvironment, Chinese Academy of Sciences, Nanjing 210008, China*
[4]*Center for Research and Education on Biological Evolution and Environment, Nanjing University, Nanjing 210023, China*
[5]*State Key Laboratory of Geological Processes and Mineral Resources, School of Earth Sciences and Resources, China University of Geosciences, Beijing 100083, China*

Correspondence should be addressed to Hua Zhang; hzhang@nigpas.ac.cn

Received 12 May 2023; Accepted 16 August 2023; Published 15 September 2023

Academic Editor: Jiyuan Yin



The tectonic evolution of the Paleo-Asian Ocean (PAO) has been well studied, including its gradual narrowing and closure by subduction. However, aspects of the tectonic evolution of the oceanic domain remain unclear, including the exact timing and nature of the closure. The Central Asian Orogenic Belt (CAOB) was formed by the closure of the PAO and, therefore, contains information about the tectonic evolution of the oceanic domain. Here, we report a study of the petrology, geochronology, and geochemistry of the Taohaiyingzi section of the Permian Linxi Formation in Alukhorqin Banner (Northeast China) in the central part of the CAOB. A newly discovered andesitic tuff from the lower part of the Linxi Formation yields a weighted mean $^{206}Pb/^{238}U$ age of 262.2 ± 1.1 Ma ($n$ = 87), indicating that the lower part of the Linxi Formation of the Taohaiyingzi section was deposited during the late Guadalupian. Provenance weathering indicators show that the sedimentary rocks of the Linxi Formation are of low maturity. Element geochemical characteristics indicate that the Linxi Formation clastic rocks were derived from eroded magmatic rocks that formed in a continental arc setting and were deposited close to the arc in a continental arc basin environment. The active margin setting was generated by the subduction of the paleo-Asian oceanic plate beneath the Xilinhot–Songliao block. The inferred palaeosalinity of the sedimentary environment changed gradually from brackish to fresh water, suggesting the end of oceanic plate subduction during the late Guadalupian, and the closure of the PAO during or after the Lopingian.

## 1. Introduction

The gradual subduction of the Paleo-Asian oceanic plate and the closure of the Paleo-Asian Ocean (PAO) during the Late Permian to Early Triassic formed a huge suture belt, namely, the Central Asian Orogenic Belt (CAOB) [1–6]. The CAOB is the largest accretionary orogenic belt in the world and is located between the Siberia–Europe plates and the North China–Tarim plates. The belt extends from the Ural Mountains in the west and passes through Kazakhstan, Kyrgyzstan, Mongolia, and Northeast China, and eastward to the west coast of the Pacific Ocean, although the eastern Nadanhada and Sikote–Alin terranes are not included [1–10]. The CAOB was formed between 600 and 250 Ma by

the convergence and subduction in different directions of multiple oceanic basins, including the Paleo-Asian oceanic basin, and is a complex collage of numerous magmatic arcs, accretionary terranes and complexes, arc-related basins, and micro-continental blocks [3–6, 11–15].

Northeast China is located in the central-eastern part of the CAOB, bordered by the North China Plate to the south and the Siberian Plate to the north. The tectonic evolution of Northeast China is complex, as the area has been influenced by the superposition of the Paleozoic PAO, Mesozoic Mongolia–Okhotsk Ocean, and Meso-Cenozoic circum-Pacific tectonic domains [1, 6, 14, 16].

Several blocks with Precambrian basement have been identified in the central–eastern part of the CAOB; that is, the Erguna, Xing'an, Xilinhot–Songliao, and Bureya–Jiamusi–Khanka blocks. At the end of the late Paleozoic, these blocks collided with the North China Plate and were amalgamated into a single composite block, following which the PAO was closed between the Siberia and North China plates (Figure 1) [6, 14, 16, 17].

The location and timing of the formation of the PAO suture are disputed. Most studies have regarded the Xar Moron–Changchun–Yanji line as the suture zone between the Siberian and North China plates [8, 18–23]. However, others have considered that the amalgamation zone of the two plates is located along the Hegenshan–Heihe fault zone [24–27]. There are also differing views on the timing of the closure of the PAO. Although some studies have proposed a Middle Devonian [25, 28] or Late Devonian to early Carboniferous [29, 30] closure, most have argued for closure during the Guadalupian–Lopingian to Early–Middle Triassic [8, 23, 31–34].

Previous studies of the tectonic evolution of the PAO have focused mainly on magmatic (including volcanic) rocks, palaeontology, and palaeomagnetism, with fewer investigating sedimentological aspects. Sedimentary systems record the weathering and denudation processes of their source area and can also provide a reliable geological record of tectonic activity and geodynamic setting. The Permian Linxi Formation in Northeast China has been extensively investigated because of its age, tectonic setting, and significance. Studies have examined the age [35–39], palaeontological evidence [40, 41], sedimentary environment [42–44], and tectonic setting [31, 45, 46] of the Lopingian Linxi Formation in the study area. Furthermore, oil and gas geological surveys have shown that the Linxi Formation has high oil and gas resource prospectivity [47, 48].

Several major biological and geological events occurred during the Permian, including the final amalgamation of Pangea. Dramatic changes in marine and continental environments eventually led to the largest extinction event in geological history at the end-Permian [49–54]. The Permian was also a period of widely variable palaeogeographic environments, meaning that comparing Permian strata from different regions is challenging. In Northeast China, many aspects of Permian strata remain uncertain, and a comprehensive timescale has not yet been constructed, thus hampering the comparison, correlation, and understanding of regional geological events. Detailed studies of critical Permian stratigraphic intervals in Northeast China would provide important constraints on the tectonic evolution of the PAO; however, such studies are lacking.

High-precision dating plays an important role in constraining stratigraphic ages and regional stratigraphic correlation [51, 52, 54]. A precise age for the Permian Linxi Formation is required to improve the regional correlation of strata and reconstruct the evolution of the PAO, including its closure. The Permian Linxi Formation was deposited during the tectonic transition between the PAO and Pacific Ocean tectonic domains. Here, we report a precise age for the Linxi Formation and analyze its sedimentary environment and tectonic setting to better constrain the evolution of the PAO.

## 2. Geological Setting

The study area is located in the Xilinhot–Songliao block of Northeast China, in Alukhorqin Banner of the Inner Mongolia Autonomous Region (Figure 2(a)). The area includes the location of the final closure of the PAO, as represented by widely exposed late Palaeozoic strata [33, 35, 36, 55–57]. Stratigraphic units in the study area include the Cisuralian Shoushangou ($P_1ss$) and Dashizhai ($P_1d$) formations, the Guadalupian Zhesi Formation ($P_2z$), and the Lopingian Linxi Formation ($P_3l$). The Shoushangou Formation is composed of clastic rocks that contain limestone lenses, with the latter containing abundant fusulinid, coral, and brachiopod fossils. The Dashizhai Formation is a marine volcano-sedimentary deposit containing suites of intermediate–felsic to intermediate–mafic volcanic rocks. A rhyolite from the Dashizhai Formation adjacent to the study area has yielded zircon U–Pb ages of 279 ± 3 Ma [58] and 292.8 ± 2.7 Ma [59]. The Zhesi Formation consists of sandstone, slate, and limestone and locally contains felsic pyroclastic rocks and abundant marine fossils. The Linxi Formation comprises sandstone, slate, and mudstone and contains fossils. Mesozoic strata are widely exposed in the study area, including the Middle Jurassic Xinmin Formation ($J_2$xm), Upper Jurassic Manketouebo Formation ($J_3$mk), Manitu Formation ($J_3$mn), and Baiyingaolao Formation ($J_3$b; Figure 2(a)). The lithologies are mainly intermediate–felsic volcanic rocks and pyroclastic rocks. Most previous studies of the Linxi Formation have focused on its lithological associations, palaeontology, and detrital zircon chronology [33, 35, 36, 40]. However, there have been no reports of volcanic rock chronology, which would provide the most reliable basis for accurately constraining the age of the Linxi Formation. The lack of such age data has hindered our understanding of the Linxi Formation and the reconstruction of the regional tectonic evolution.

The Taohaiyingzi section is located in Baiyintala town, Alukhorqin Banner (Figure 2(a)). The section extends from 44°24'55.06"N, 120°14'00.08"E to 44°25'08.90"N, 120°13'26.88"E. The strata of the section dip northwest at 50°. The section is 950m long and 702m thick, and its base is


FIGURE 1: Fundamental palaeotectonic units of Eurasia (modified after Liu et al. [16]). The rectangle shows the study area.

obscured by Quaternary sediments. It is divided into upper and lower parts. The lower part comprises a set of gray–black mudstone and gray–green sandstone. The upper part contains interbedded fine-grained sandstone and mudstone. Cross-bedding, wavy cross-bedding, and ripple marks are developed in the sandstone. The feldspathic lithic sandstone has low compositional maturity, indicating that the study area lay close to the provenance area. In 1996, the Inner Mongolia Bureau of Geology and Mineral Resources classified the Taohaiyingzi section as one of the representative sections of the Linxi Formation. Fossils of sporopollen, spinicaudatans, bivalves, and plants have been collected from several horizons in the lower part of the Taohaiyingzi section, on which basis a Lopingian age has been assigned [60].

In this study, an andesitic tuff interlayer was discovered in the upper part of the Taohaiyingzi section and was dated using U–Pb zircon geochronology. Samples were collected from the section for geochemical analysis, and previously published geochemical data were incorporated from clastic rocks of the section and well TD1 (Table S2). This borehole was drilled into Permian rocks for petroleum and natural gas exploration. Well TD1 is located 100m from the section and intersects the same layers of the Linxi Formation as those exposed in the upper part of the Taohaiyingzi section (Figures 2 and 3); fresh mudstone samples were obtained from well TD1.

## 3. Samples and Methods

Foursamples of volcanic rock and eight samples of clastic rocks were collected from the Taohaiyingzi section for zircon isotope dating and geochemical analyses, respectively. Samples for geochemical analysis were collected from beds 32 to 56 of the section and are composed of fine gray sandstone and gray–black mudstone. Data from previous studies of the section are also referred (e.g., Zhen et al., 2018; Zhang et al., 2019b; Table S1).

*3.1. U–Pb Zircon Geochronology of Volcanic Rock.* The dated sample (ABP1-51TWS) is an andesitic tuff collected from Bed 51 of the studied section (Figure 3). The tuff occurs as an interlayer in black mudstone and is 15–20cm thick (Figures 4(a)–4(c)).

The andesitic tuff is massive and consists mainly of tuffaceous and interstitial sedimentary material. Crystal fragments are 0.3–1.2mm long and comprise plagioclase and quartz. Plagioclase fragments constitute 77vol% of the tuff, with most being subidiomorphic and some being

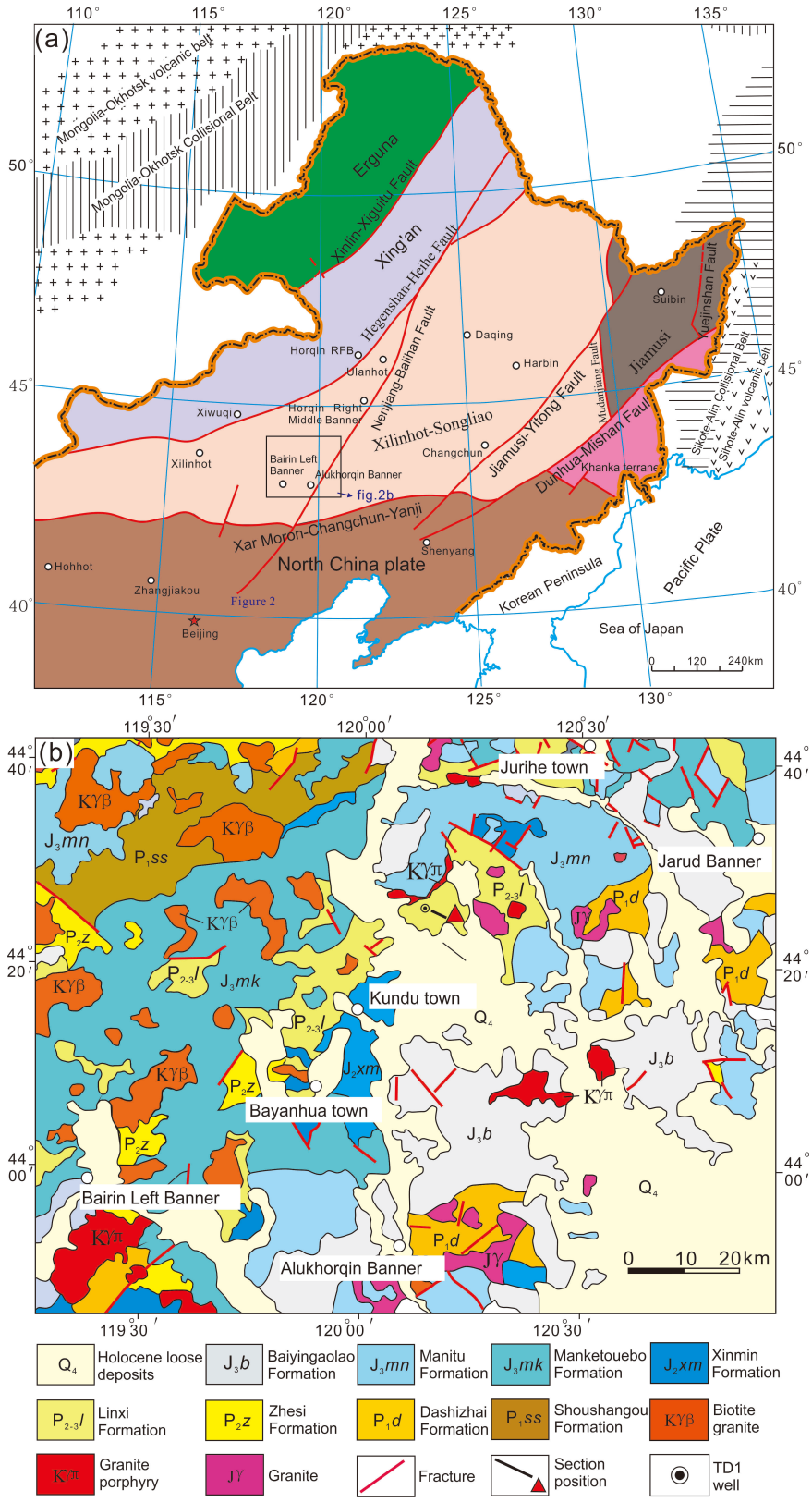


FIGURE 2: (a) Simplified geological map of Northeast China, showing geological tectonic units (modified after Sun et al. [114]). (b) Geological map of Alukhorqin Banner in Northeast China, showing the locations of the Taohaiyingzi section and well TD1 (modified after Zhang et al. [73]).

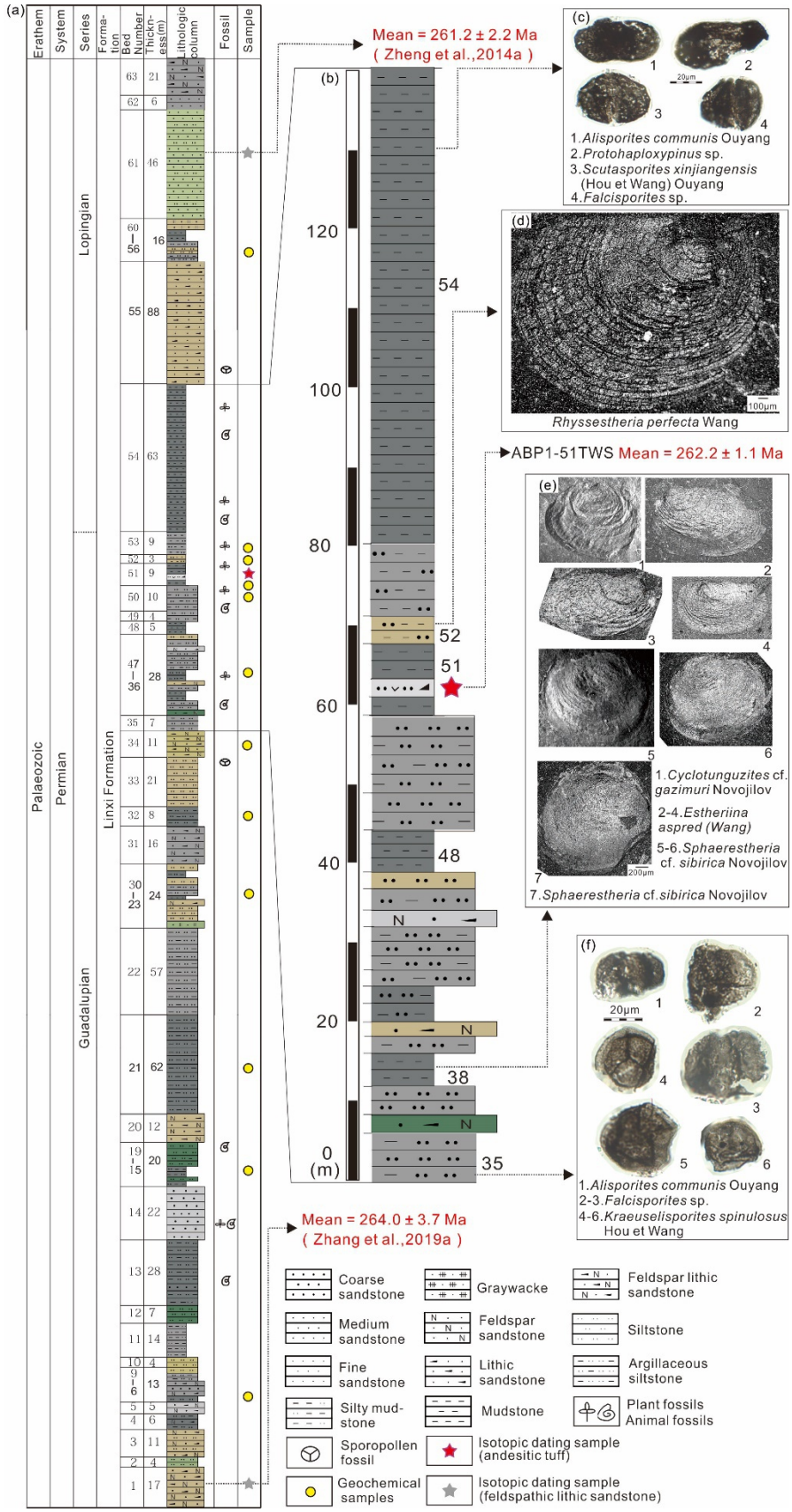


FIGURE 3: (a–b) Stratigraphic section of the Permian Linxi Formation ($P_{2\text{-}3}l$) at Taohaiyingzi. (c) Sporopollen fossils reported by Zheng et al. [35]. (d–e) Estheria fossils reported by Zheng et al. [35]. (f) Sporopollen fossils reported by Zheng et al. [35].

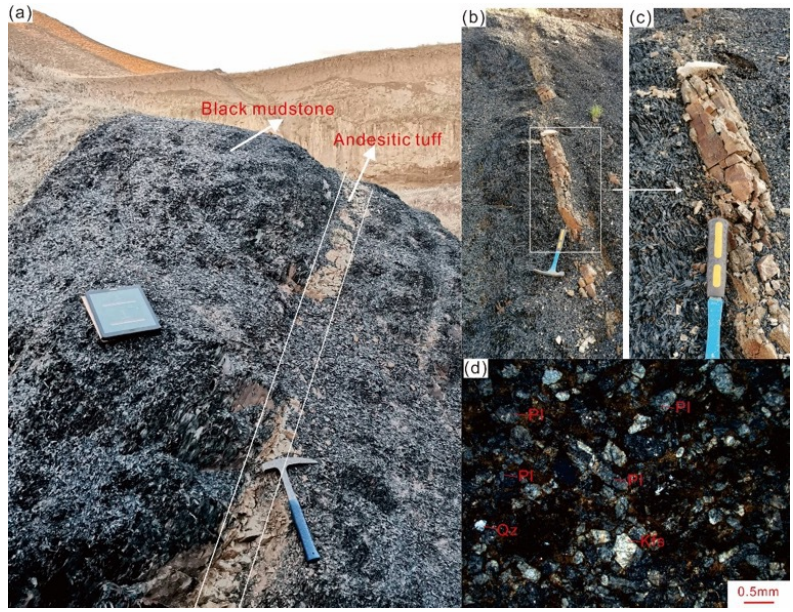


Figure 4: Field photographs and petrographic characteristics of the sample obtained for zircon U–Pb dating (ABP1-51TWS). (a–c) Field occurrence of andesitic tuff. (d) Characteristics of andesitic tuff under the microscope.

sericitized. Quartz fragments constitute 3vol% of the tuff and are subangular and fractured. The rock debris consists of graphic granite composed of K-feldspar and quartz. Sedimentary interstitial material includes recrystallized clay minerals (Figure 4(d)).

Zircon crystals were extracted from a whole-rock sample of andesitic tuff using combined standard magnetic and heavy liquid separation techniques at the Langfang Chengxin Geological Service Company, Langfang, China. Selected zircons were examined under both transmitted and reflected light using an optical microscope. Crystals free of major fractures and visible inclusions were handpicked, mounted in epoxy resin, and then polished to expose their centers. Cathodoluminescence (CL) images were obtained using a CL spectrometer (Garton Mono CL3+) attached to a scanning electron microscope (Quanta 200F) with a 2-min scanning time operated at 15 kV and 120 nA at Peking University, Beijing, China. Distinct domains within the zircons identified in CL images were selected for analysis (Figure 5). U–Pb geochronological analysis employed a quadrupole inductively coupled plasma–mass spectrometer (ICP–MS; Agilent 7500a) equipped with a UP-193 solid-state laser (193 nm, New Wave Research), housed at the Geologic Laboratory Center, China University of Geosciences, Beijing, China. Analyses employed a laser energy density of 8.5 J/cm$^2$, repetition rate of 10Hz, and beam diameter of 36μm. The ablated material was carried into the ICP–MS by a high-purity He gas stream with a flux of 0.8 L/min. Zircon 91,500 was used as the external standard, and the standard silicate NIST 610 glass was used for instrument optimization [61]. Zircon standards TEMORA [62], Qinghu [63], and GJ-1 [64] were used as secondary standards to monitor age measurements, and common Pb was corrected following Andersen [65]. Standards 91,500, GJ-1, and Qinghu zircons were analyzed after every ten unknowns. Analysis of each block of five unknowns was followed by analysis of these threestandards, with each analysis involving a 30s blank measurement followed by a further 40s of measurement during ablation. The weighted mean $^{206}Pb/^{238}U$ ages for 91,500 and GJ-1, as obtained in this study, are 1063.1 ± 5.8 Ma (2σ, $n$ = 32) and 600.7 ± 5.4 Ma (2σ, $n$ = 8), consistent with the recommended values within analytical uncertainties [64, 66]. Isotopic ratios and element contents were calculated using GLITTER (version 4.4, Macquarie University). Age calculations and concordia plots were completed using Isoplot (ver 3.0) [67].

*3.2. Analysis of Major, Trace, and Rare Earth Elements.* Samples of clastic rocks for geochemical analysis were collected from Beds 6to57 of the section, and samples of volcanic rocks were collected from Bed 51. The clastic rocks are composed mainly of gray feldspathic lithic sandstone, gray–black siltstone, and black mudstone. The volcanic rock is gray–yellow andesitic tuff.

Major oxide compositions were analyzed using a PANalytical Axios Advance (PW4400) X-ray fluorescence spectrometer at the Northeast China Supervision and Inspection Center of Mineral Resources, Ministry of Natural Resources, Shenyang, China. Loss on ignition was measured using 1g of powder heated to 1100°C for 1hour. Major oxides were analyzed in fused glass with an uncertainty of <2%.

Trace element and rare earth element (REE) compositions were measured using a PerkinElmer SCIEX ELAN 6000 ICP instrument at the Northeast China Supervision and Inspection Center of Mineral Resources, Ministry of Natural Resources. The powdered samples were dissolved in a mixture of $HNO_3$ + HF in a high-pressure Teflon bomb for 48hours at 190°C [68]. Rhodium was used as an internal standard to monitor instrumental drift during

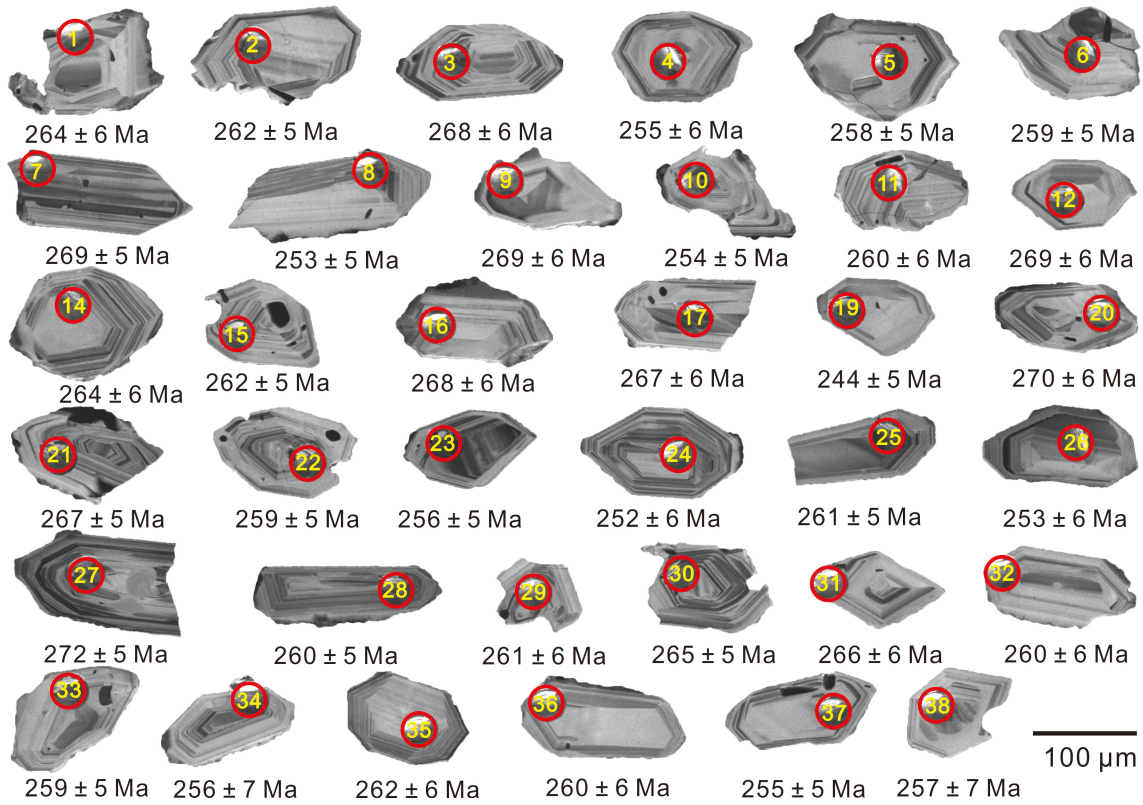


FIGURE 5: CL images and $^{206}Pb/^{238}U$ ages of analyzed zircons from the andesitic tuff. Red circles indicate analytical spots for U–Pb dating.

counting, and the international standard GBPG-1 was used for quality control. Measurement results of international standards OU-6 and GBPG-1 were in agreement with the recommended values. The analytical uncertainty for all element contents was <5%.

## 4. Analytical Results

*4.1. Geochronology.* Laser ablation–ICP–MS U–Pb isotope analysis was performed on 98 zircons from the sample of andesitic tuff. CL images reveal that most zircons are euhedral to subhedral and show the crystal form of typical magmatic zircon (Figure 5). The zircons have grain sizes of 90–150μm, aspect ratios of ~2:1, and magmatic oscillatory zoning, with Th/U ratios of 0.23–1.87 (mean of 0.55), indicating a magmatic origin (Figure 5).

The results for the analyzed zircons (Figure 6(a)) show that 87 of the age data fall on the concordia. The weighted mean age of 87 data (excluding eleven spots with a concordance of <95%) is 262.2 ± 1.1 Ma (Mean Square of Weighted Deviates (MSWD) = 0.89; Figures 6(a) and 6(b); Table S1), indicating a late Guadalupian age for the andesitic tuff.

*4.2. Geochemical Analyses*

*4.2.1. Major Oxides of Clastic Rocks and Volcanic Rocks.* The $SiO_2$ contents of the sampled sandstone and mudstone range from 63.73 to 67.89wt%, with a mean of 66.49wt%. $Al_2O_3$ contents range from 10.49 to 16.72wt% (mean of 15.32wt%; Figure 7). Other major oxide contents include $TiO_2$ (0.39, 0.73wt%, mean of 0.63wt%), FeO (1.16, 4.61wt%, and mean of 2.13wt%), total $Fe_2O_3$ (2.84, 5.26wt%, and mean of 3.97wt%), MgO (1.13, 2.47wt%, and mean of 1.49wt%), CaO (0.47, 0.96wt%, and mean of 0.68wt%), $Na_2O$ (0.32, 2.30wt%, and mean of 1.62wt%), and $K_2O$ (1.44, 3.73wt%, and mean of 3.06wt%). Values of $K_2O/Na_2O$ range from 1.26 to 4.52, and $Al_2O_3/(CaO + Na_2O)$ values range from 5.78 to 10.58. Contents of $SiO_2$, $Al_2O_3$, MgO, $P_2O_5$, MnO, and $TiO_2$ vary within a narrow range, whereas those of $Na_2O$, $K_2O$, and CaO have wider ranges (Figure 7). $Al_2O_3$ correlates positively with $Fe_2O_3$ and $K_2O$, negatively with $SiO_2$ and $Na_2O$, and shows no relationship with $TiO_2$ (Figure 7; Table S2). These results indicate that the samples have undergone negligible late alteration [69]. The high content of total $Fe_2O_3$ + MgO (4.0, 7.6wt%, and mean of 5.5wt%) reflects the abundant siliceous minerals in the samples, implying that these clastic rocks have low maturity and that the source area may have comprised rocks from a volcanic arc [70].

Geochemical analysis was conducted for four volcanic rock samples. The $SiO_2$ contents of the andesitic tuff range from 57.56 to 58.47wt%, with a mean of 58.09wt%. The tuff is enriched in aluminum, and $Al_2O_3$ contents range from 24.67 to 25.18wt% (mean of 24.85wt%). The rocks are rich in alkalis ($Na_2O + K_2O$ = 7.79–8.20wt%, mean of 7.99wt%). The contents of other major elements are relatively low: CaO (0.99, 1.04wt%, and mean of 1.01wt%), $TiO_2$ (0.80, 0.87wt%, and mean of 0.85wt%), total $Fe_2O_3$ (3.16, 4.10wt%, and mean of 3.81wt%), and MgO (1.36, 1.48wt%, and mean of 1.41wt%). In a total-alkalis–silica

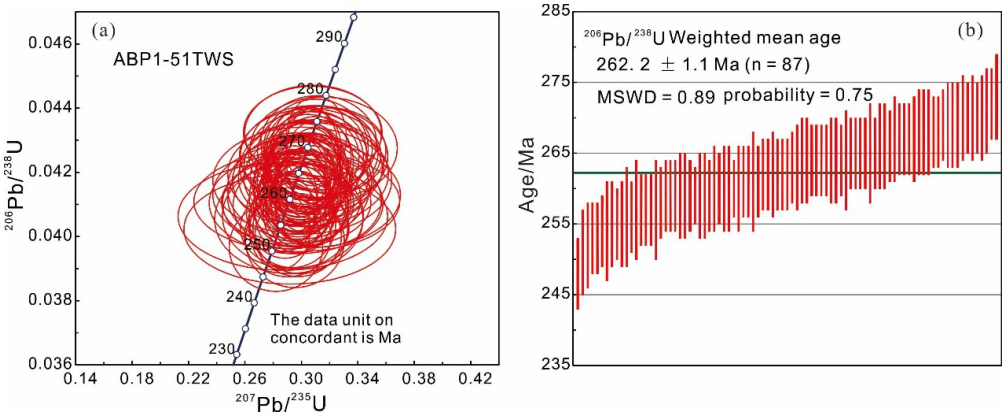


Figure 6: (a) Zircon U–Pb concordia diagram and (b) weighted mean age diagram for the andesitic tuff. The weighted mean $^{206}Pb/^{238}U$ age for zircon standard 91,500 was 1063.1 ± 5.8 Ma (2σ, $n$ = 32).

diagram, the samples fall in the trachyandesite field (Figure 8(a)). In an $SiO_2$ versus Nb/Y diagram, the samples plot in the andesite field (Figure 8(b)). In a $K_2O$ versus $SiO_2$ diagram (Figure 8(c)), the samples are classified as shoshonite series.

*4.2.2. Trace Elements.* The analyzed sandstone and mudstone have similar contents (Table S2) of high-field-strength elements (HFSEs; e.g., Nb, Ta, Zr, Hf, P, Th, Ce, U, and Ti) and are enriched in large-ion lithophile elements (LILEs; e.g., K, Rb, Cs, and Ba; Figure 9(a)). The contents of the LILEs Rb, Sr, Cs, Ba, and U are 63.2–137, 108–144, 4.94–20.7, 309–696, and 2.7–4.5 μg/g, respectively (Table S2). The contents of Cs, Ba, and U are similar to those of post-Archean Australian shale (PAAS) [71], whereas the contents of K and Sr are lower. $Al_2O_3$ displays a positive correlation with Rb but no clear relationship with Cr (Figure 7), suggesting that clay minerals are not the only control on the contents of these elements [72].

The clastic rock samples have similar patterns of REE contents, with similar mean abundances ranging from 156 to 192μg/g and a mean of 176μg/g, similar to the value for PAAS. All of the samples are enriched in light REEs (LREEs) [$(La/Yb)_N$ = 5–6] and have relatively flat HREE patterns (Figure 9(b)). The samples have marked negative Eu anomalies (Eu/Eu* = 0.48–0.61), slight negative Ce anomalies (Ce/Ce* = 0.87–0.96), and moderately differentiated REE patterns, with LREE/HREE ratios of 4.38–6.71 (mean of 5.93).

The four andesitic tuff samples are enriched in LILEs (e.g., Ba, U, K, and Sr) and depleted in HFSEs (e.g., Nb, Ta, Zr, and Ti; Figure 9(c)). These samples yield similar patterns of REE contents, with similar mean abundances of 84.45–93.45μg/g and a mean of 89.81μg/g. The samples are enriched in LREEs [$(La/Yb)_N$ = 12.78–16.15] and show depleted HREE patterns (Figure 9(d)). They have negative Eu anomalies (Eu/Eu* = 0.70–0.78), positive Ce anomalies (Ce/Ce* = 1.14–1.29), and clearly differentiated REE patterns, with LREE/HREE ratios of 8.88–10.79 (mean of 9.76). The rare earth and trace element characteristics of the andesitic tuff are clearly different from those of sandstone and mudstone.

## 5. Discussion

### 5.1. Age of the Linxi Formation

*5.1.1. Age of the Analyzed Andesitic Tuff.* The andesitic tuff in the fine clastic rocks of the Taohaiyingzi section provides an opportunity to precisely date the Linxi Formation. Our zircon U–Pb dating of the tuff (sample ABP1-51TWS; Figure 6) provides highly consistent results for a large number of determinations ($n$ = 87) and gives a formation age of 262.2 ± 1.1 Ma for the tuff. The age of the Linxi Formation in Northeast China has not been well constrained in previous studies owing to the lack of volcanic rocks that can be accurately dated. The newly discovered tuff in this study is the first reported volcanic rock from the Linxi Formation, and its age precisely defines the age of the Linxi Formation in the Taohaiyingzi section. Accordingly, we infer that the lower part of the Linxi Formation in the Taohaiyingzi section was deposited during the late Guadalupian.

*5.1.2. Constraints on the Depositional Age of the Linxi Formation.* Previous studies have investigated the age of the Linxi Formation using palaeontology and isotope geochronology. The Linxi Formation is widely distributed in the Great Xing'an Range area and was previously assigned to the Lopingian on the basis of assemblages of estheria, plants, and bivalve fossils. Abundant bivalves and plant fossils occur in the Taohaiyingzi section, including *Pecopteris*, *Rhipidopsis*, *Callipteris*, *Compsopteris*, and *Schizoneura manchuriensis* [40, 60]. The bivalves are part of the *Palaeonodonta–Palaeomutela* assemblage, dated as Lopingian [40]. Wang [60] reported estheria from this section, including *Palaeolimnadia* cf. *glabra*, *P. rossica*, *Costestheria taohaiyingziensis*, *C. scoliogabata*, *Pemphicyclus baiyintalaensis*, *P. trochoides*, *P.* cf. *arangastachus*, *Palaeolimnadiopsis deminuta*, *Rhyssestheria lampra*, *R. perfecta*, *Sphaerestheria* cf. *sibirica*, and *Estheriina aspred*, which are Lopingian in age. Zheng et al. [35] studied estheria, sporopollen, and other fossils from the middle and lower parts of the Taohaiyingzi section. Fossils are from beds 35, 38, 48, 52, 53, and 54 of the section, and the

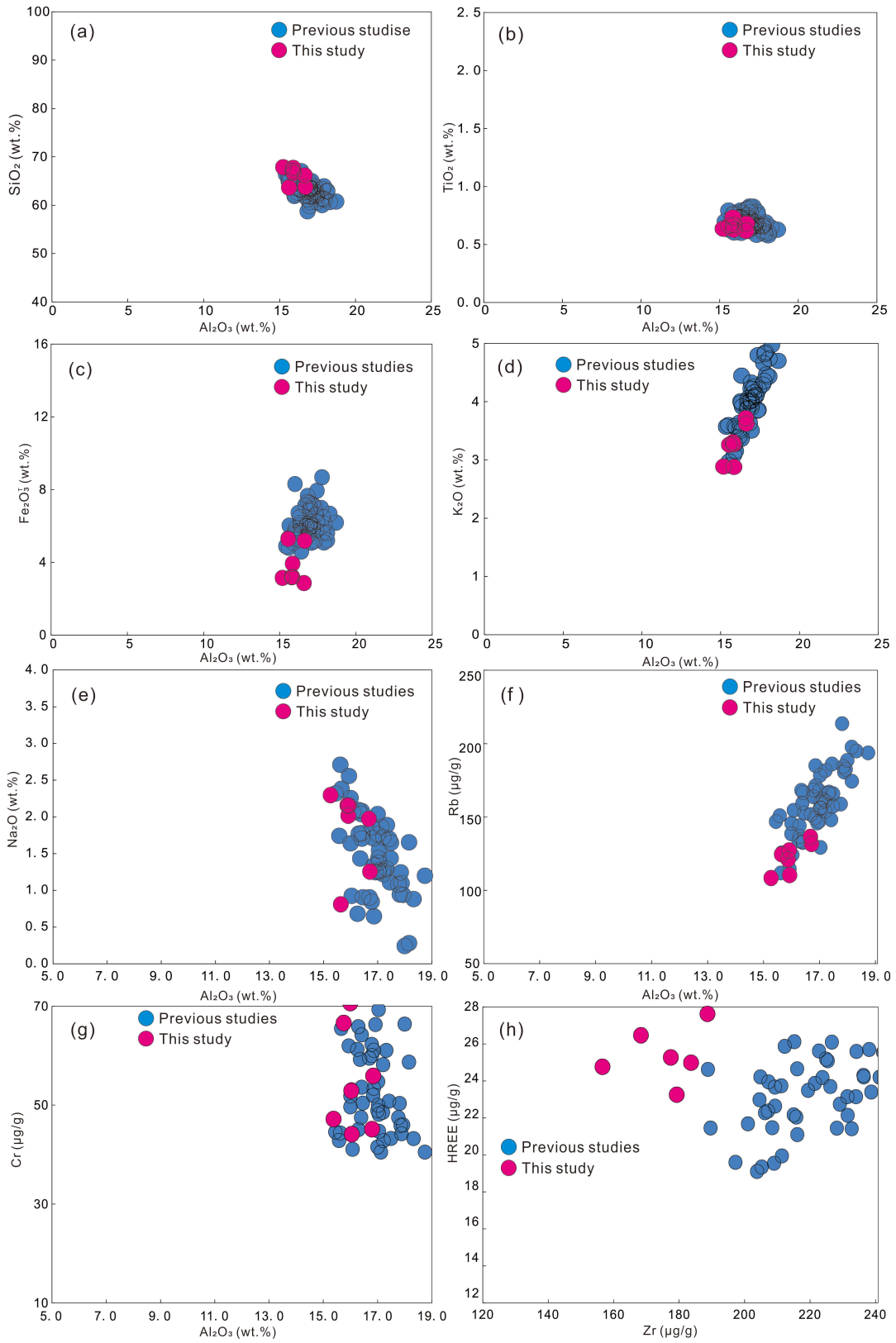


FIGURE 7: Diagrams of major and trace element contents versus $Al_2O_3$, and heavy rare earth elements (HREEs) versus Zr. (a) $SiO_2$ versus $Al_2O_3$, (b) $TiO_2$ versus $Al_2O_3$, (c) $Fe_2O_3$ versus $Al_2O_3$, (d) $K_2O$ versus $Al_2O_3$, (e) $Na_2O$ versus $Al_2O_3$, (*f*) Rb versus $Al_2O_3$, (g) Cr versus $Al_2O_3$, and (h) HREEs versus Zr. Previous data are from Zhang et al. [104] and Zhen et al. [105].

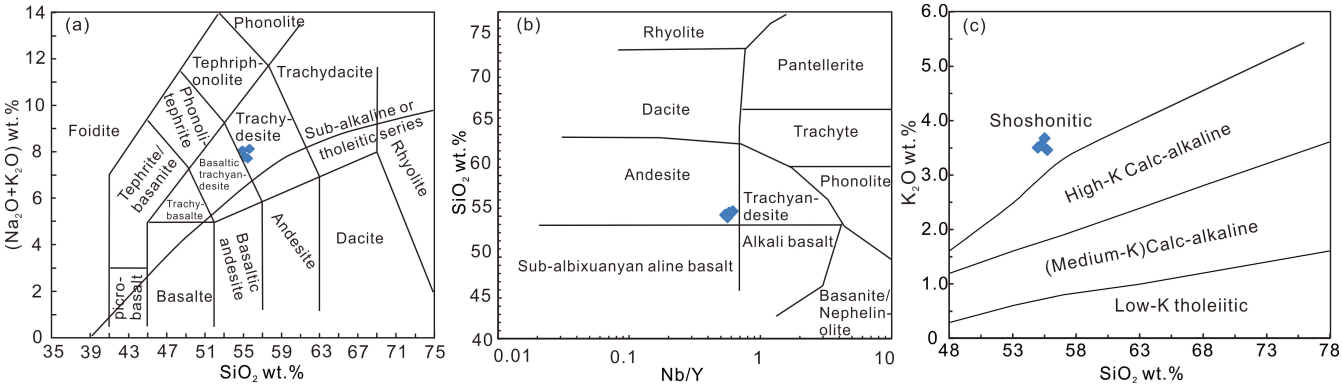


FIGURE 8: Classification diagrams for andesitic tuff from the Linxi Formation. (a) Total alkalis versus $SiO_2$ (after Le Maitre [115]); (b) $SiO_2$ versus Nb/Y (after Winchester and Floyd [116]); (c) $K_2O$ versus $SiO_2$ (after Peccerillo and Taylor [117]).

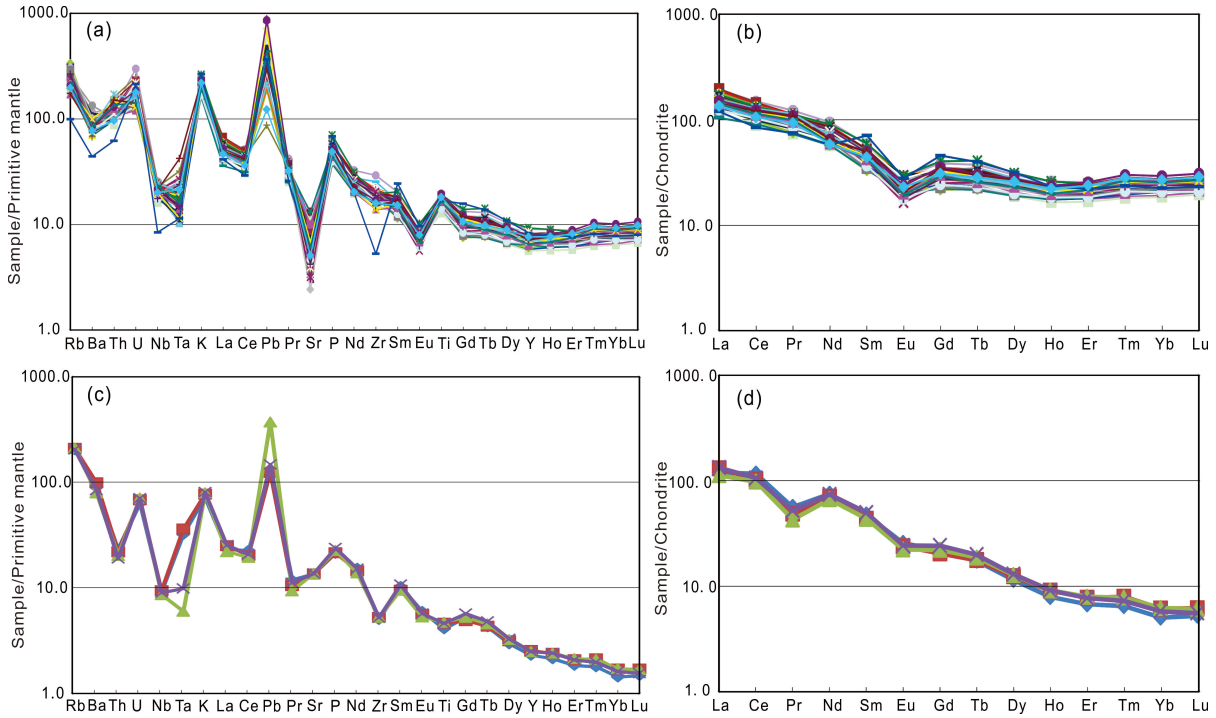


FIGURE 9: Trace element and REE variation diagrams for the Taohaiyingzi section of the Linxi Formation in Alukhorqin Banner. (a) Primitive-mantle-normalized trace element spider diagram for clastic rocks; (b) chondrite-normalized REE patterns for clastic rocks; (c) primitive-mantle-normalized trace element spider diagram for andesitic tuffs; (d) chondrite-normalized REE patterns for andesitic tuffs. Chondrite normalization values are from Boynton [118], and primitive mantle normalization values are from Sun and McDonough [119].

newly discovered estheria are *Cyclotunguzites* cf. *gazimuri* Novojilov *and Pseudestheria* sp. The estheria *Cyclotunguzites* is representative of assemblages from the Guodikeng Formation. The Guodikeng Formation is located in the Junggar Basin and belongs to the Lopingian, with Lopingian fossils. Sporopollen fossils include *Alisporites communis*, *Falcisporites* sp., *Protohaploxypinus* sp., *Scutasporites xinjiangensis*, and *Kraeuselisporites spinulosus*. It is considered that the Linxi Formation exposed in the Taohaiyingzi section can be correlated with the Wutonggou Formation and the middle and lower parts of the Guodikeng Formation exposed in the Dalongkou section at Jimusar, Xinjiang, which are generally acknowledged as being equivalent to the late Wuchiapingian–Changhsingian (Figure 3). Zhang et al. [41] reported that the middle and upper parts of the Guandi section, which is located ~150 km southwest of the Taohaiyingzi section, also contain Lopingian estheria fossils. The abovementioned palaeontological and stratigraphic findings show that the age of deposition of the upper part of the Linxi Formation in the study area was Lopingian.

Zheng et al. [36] performed U–Pb detrital zircon dating of a feldspathic lithic sandstone sample from the Linxi Formation in the Taohaiyingzi section (Bed 1) and obtained a youngest peak age of 261 Ma (Figure 3). The youngest group of zircons from the sandstone at the bottom of the section ranges in age from 301 to 248 Ma ($n$ = 40), accounting for 42% of the total number of grains. Wang et al. [57] conducted SHRIMP U–Pb dating of zircon from feldspar lithic sandstone from Bed 1 of this section, which yielded a weighted mean age of 260.7 ± 1.2 Ma (MSWD = 1.13, $n$ = 13), with the youngest zircon age of 256.0 ± 2.5 Ma, which may represent the maximum depositional age of the Linxi Formation at this locality. Zhang et al. [73] performed U–Pb isotopic dating of zircon from feldspathic lithic sandstone from Bed 61 of the section and obtained a peak age of 263 Ma ($n$ = 41) for the youngest group of detrital zircons. The youngest group of zircons, ranging in age from 302 to 250 Ma, accounts for 41% of the total number of grains. Twodetrital zircon sample ages previously published for the section [36, 73] were reprocessed in this study, involving the re-screening and analysis of data, and yielded weighted mean ages of 264.0 ± 3.7 and 261.2 ± 2.2 Ma, respectively (Figure 3). Combining these previous ages for detrital zircons from the Taohaiyingzi section gives a stratigraphic age of 264.2 ± 3.4 to 256 ± 2.5 Ma, which is consistent with our age of 262.2 ± 1.1 Ma for the andesitic tuff.

Previous studies have investigated the ages of detrital zircons from the Linxi Formation in other sections of Northeast China. Han et al. [33] dated zircons from clastic rocks in the Linxi area and obtained maximum depositional ages of 278 and 250 Ma from twosites. Han et al. [74] conducted zircon U–Pb dating of zircon from the Linxi Formation sandstone in the Linxi area and determined a maximum depositional age of 256 Ma. Song et al. [75] dated detrital zircons from the sandstones of the Zhesi Formation in the Xiwuqi area, Inner Mongolia, giving a maximum depositional age of 263 Ma. Zhang et al. [56] conducted detrital zircon isotope dating of Linxi Formation samples from Bairin Left Banner of Inner Mongolia and obtained a maximum depositional age of 266 Ma. Finally, Chen et al. [76] dated detrital zircons from the Linxi Formation in Horqin Right Middle Banner, Inner Mongolia, and proposed a maximum depositional age of 263 Ma. In summary, the age of detrital zircons of the Linxi Formation from the Taohaiyingzi section is consistent with the ages determined in the Linxi, Bairin Left Banner, and Horqin Right Middle Banner areas within the range of errors of detrital zircon ages. However, there is a wide range in estimates of the maximum depositional age based on detrital zircon chronology, with ages of 278–250 Ma, although most lie between 266 and 256 Ma.

In summary, fossil assemblages, detrital zircon dating, and regional geological data indicate that the Linxi Formation has an extensive distribution. The tuff sample obtained from the Taohaiyingzi section in this study yielded an age of 262.2 ± 1.1 Ma, which is the first direct (i.e., nonpalaeontological and nondetrital zircon) age for the Linxi Formation in the study area. Our zircon U–Pb dating of the andesitic tuff of the Taohaiyingzi section establishes the initiation of deposition of the Linxi Formation as no later than 262.2 ± 1.1 Ma.

*5.2. Sedimentary Environment and Provenance of the Linxi Formation.* The source rocks of the Linxi Formation are likely to have been variable and complex, and the potential effects of sedimentary differentiation, recycling, further weathering in the provenance area, and metasomatism during diagenesis should be considered when undertaking a quantitative analysis of the intensity of palaeoweathering and palaeoclimate in the source area.

Silica in clastic sedimentary rocks is contributed mainly by quartz particles, and $Al_2O_3$ is contributed mostly by feldspar and clay minerals, meaning that the $SiO_2/Al_2O_3$ ratio can be used to reflect the maturity of sedimentary rocks. With increasing quartz content and decreasing feldspar and clay mineral contents, the $SiO_2/Al_2O_3$ ratio increases, reflecting an increase in maturity [77]. The mean $Al_2O_3$ content of the studied samples is relatively high (mean of 15.32 wt%), and $SiO_2/Al_2O_3$ is relatively low (mean of 4.4), implying that the clastic rocks in the Taohaiyingzi section have low maturity. Clastic rocks from the section are interpreted to be the products of near-source and rapid sedimentation.

The REE contents of clastic rocks are determined mainly by the compositions of rocks in the provenance region. REEs are insoluble and have very low concentrations in water, and they are instead transported in the form of lithic fragments and are less affected by diagenetic processes. Patterns of REE contents can faithfully reflect the nature of the source area, meaning that they can be used as important tracers of provenance [71, 78–82]. The chondrite-normalized REE patterns of the studied clastic rocks are highly consistent, showing LREE enrichment, uniform and slightly depleted HREE contents, and negative Eu anomalies (Figure 9(b)). This pattern is consistent with that of post-Archean REEs in the upper crust, indicating that the source rocks of the Linxi Formation sedimentary rocks were derived from the upper crust. The trace element contents of the samples also have similar patterns (Figure 9(a)), characterized by depletion in Nb, Ta, and Sr, and enrichment in Rb, Ba, La, Ce, Pb, Nd, and Sm, suggesting that the Linxi Formation sedimentary rocks were derived mainly from felsic rocks.

Previous studies have shown that high Rb/Sr values for sedimentary rocks indicate warm and humid environments, whereas low Rb/Sr values indicate dry and cold environments [83]. The studied samples display high Rb/Sr ratios of 0.46–3.86, with a mean of 1.35, which is higher than the average PAAS (~0.8 [71]), indicating warm and humid climatic conditions. During weathering, U is more mobile than Th. With increasing intensity and/or duration of chemical weathering, U tends to be oxidized and therefore depleted, meaning the Th/U ratio increases [71, 84, 85]. The mean Th/U value of the samples is 2.8, which is lower than the upper continental crust (UCC) value of 3.8 [71], suggesting weak chemical weathering in the provenance area. In addition, the samples show broadly parallel patterns

in spider diagrams (Figure 9), implying that the rocks have retained the original REE and HFSE characteristics, or probably had a uniform source area, meaning that the element content patterns can be reliably used to trace the provenance and tectonic setting of the clastic rocks.

An $Al_2O_3$–($CaO+Na_2O$)–$K_2O$ (A–CN–K) diagram can be used to investigate the weathering, metasomatism, and provenance of clastic rocks [86, 87]. Under ideal conditions, data are distributed parallel to A–CN or A–K in such a diagram [88], whereas metasomatic processes will result in the data deviating from either of these directions, with greater deviation signifying stronger metasomatism. In the A–CN–K diagram of Figure 10(a) , the data are distributed mostly parallel to A–CN, suggesting that metasomatism of the samples after deposition was weak. We propose that the geochemical characteristics of the clastic rocks of the Linxi Formation have been negligibly affected by late diagenesis or metamorphism, and therefore, weathering was the main control on the geochemical compositions of the rocks, thereby allowing them to be used for the study of provenance and weathering.

Source weathering is a key influence on the chemical and mineral composition of clastic sedimentary rocks. The chemical index of alteration (CIA) can be used to measure the degree of chemical weathering in the source area [89]. It is considered that the CIA value can be used to infer the chemical weathering intensity and palaeoclimate during the period of sedimentation, as follows [90, 91]: CIA values of 50–65 reflect a low intensity of chemical weathering under cold and dry climatic conditions; CIA values of 65–85 represent a moderate intensity of weathering under warm and humid climatic conditions; and CIA values of 85–100 reflect intense weathering under hot and humid tropical and subtropical climatic conditions. CIA values measured for the studied mudstones of the Linxi Formation range from 60.0 to 80.3, with a mean of 66.7 (Figure 10(b); Table S2), suggesting that the provenance was affected by moderately intense chemical weathering under warm and humid climatic conditions, consistent with the environmental characteristics inferred from Rb/Sr values.

The index of chemical variation (ICV) can be used to determine the chemical composition of the source area [70]. Clastic rocks with ICV values of <1 are generally derived from sources containing abundant clay minerals, indicating recycling in an active tectonic setting or intense weathering. Clastic rocks with ICV values of >1 indicate primary deposition in an active tectonic setting [92, 93]. The ICV values of the studied samples indicate that they are composed of immature sedimentary rocks (Figure 10(b)), with values of 1.01–1.23 (mean of 1.09) indicating that the rocks were derived mainly from immature source areas in an active tectonic regime. In addition, higher ICV values may indicate sediment from the first cycle of deposition (i.e., not recycled) in an active tectonic setting [94–97]. This inference is consistent with the conclusion based on the major oxide data that the source was situated adjacent to the depositional area, and the sediments were rapidly accumulated. In a $TiO_2$–Ni diagram (Figure 11(a)), almost all of the samples fall in the felsic magmatic rock field, and most plot far from the mature sedimentary rock field, which also implies that the sediments were derived from an immature source area.

Source-rock properties have important controls on the chemical composition of sedimentary rocks [98]. Intermediate–felsic rocks have higher values of $K_2O$, Rb, and $Al_2O_3/TiO_2$, and lower values of $TiO_2/Zr$ compared with mafic rocks [99–101]. The mean $K_2O$ content of the studied rocks from the Taohaiyingzi section is 3.06wt% (Table S2), which is higher than that of the average crust (1.81wt%) and slightly higher than that of the UCC (2.8wt%) [102]. The mean content of Rb for the studied rocks is 116 ppm (Table S2), which is much higher than that of the average crust (49 ppm) and upper crust (82 ppm; [102]). In a $K_2O$–Rb diagram (Figure 11(b)), the data are clustered and fall in the intermediate–felsic composition domain, indicating that the source rock was of this composition.

$Al_2O_3/TiO_2$ ratios of sedimentary rocks can be used to infer provenance characteristics. $Al_2O_3/TiO_2$ ratios of <14 suggest that the provenance was composed of mafic rocks, and ratios of 19–28 suggest that the provenance may correspond to granodiorite and tonalite (or andesite and rhyolite) [103]. $Al_2O_3/TiO_2$ ratios for sedimentary rocks from the Taohaiyingzi section range from 21.73 to 27.22 [104, 105], indicating that granodiorite and rhyolite were probably the main constituent rocks of the source area. In an A–CN–K diagram (Figure 10(a)), the sample data are distributed along the line of granitoids, further indicating that the source area was granitic. All of the samples exhibit negative Eu anomalies, similarly suggesting that they were derived from eroded felsic rocks. Magmatic and volcanic rocks related to plate subduction during the late Palaeozoic may thus have been the main provenance.

In summary, the studied clastic rocks from the Linxi Formation represent primary deposition mainly from an immature area of felsic rocks, with rapid accumulation in an active tectonic environment.

*5.3. Implications for the Tectonic Evolution of the PAO.* Trace elements in terrigenous clastic rocks show more uniform contents compared with major elements. Elements Cr, Co, Th, Sc, La, and Zr generally display consistent patterns within the same sedimentary setting and can therefore be used to determine the nature of the source area and the tectonic setting [106]. In Th–Sc–Zr/10 and La–Th–Sc diagrams (Figure 12; [107]), data for the studied samples lie within the continental arc field, indicating that the provenance of the Linxi Formation in the study area was dominated by an active continental margin, in turn suggesting that the Linxi Formation was deposited in a back-arc basin close to a continental arc.

The andesitic tuff is enriched in LILEs (e.g., Ba, U, and K) and depleted in HFSEs (e.g., Nb, Ta, and Ti; Figure 9(c)), which are similar features to those of volcanic rocks from subduction zones [108]. In La/Yb versus Th/Yb and Th/Yb versus Nb/Y diagrams, the sample data are distributed in (or very close to) the continental arc field (Figure 13).

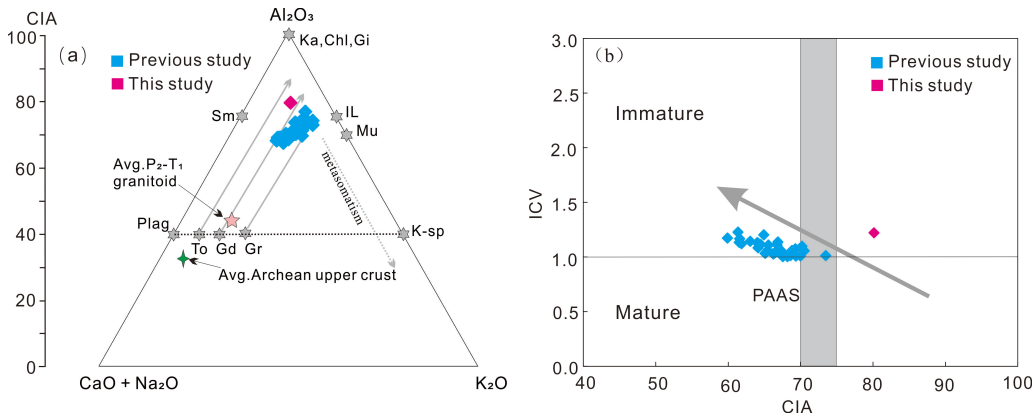


Figure 10: (a) A–CN–K diagram for clastic rocks of the Linxi Formation (after Fedo et al. [86]; Long et al. [94]). Data from previous studies are from Zhang et al. [104] and Zhen et al. [105]. (b) ICV versus CIA diagram for clastic rocks of the Linxi Formation (after Nesbitt and Young [90]; Cox et al. [70]; Long et al. [94]). The gray field represents the range of CIA values of Phanerozoic shale. CIA values of 50 and 100 correspond to fresh primary igneous rocks and the most intensely weathered rocks, respectively (Fedo et al. [86]).

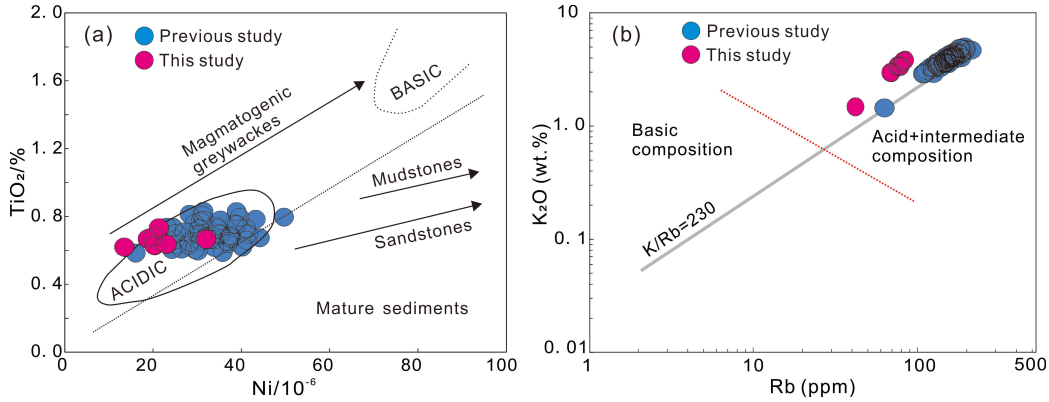


Figure 11: Source compositions for Permian clastic rocks of the Linxi Formation. (a) $TiO_2$–Ni diagram (after Floyd et al. [120]); (b) $K_2O$–Rb diagram (after Floyd et al. [99]). Data from previous studies are from Zhang et al. [104] and Zhen et al. [105].

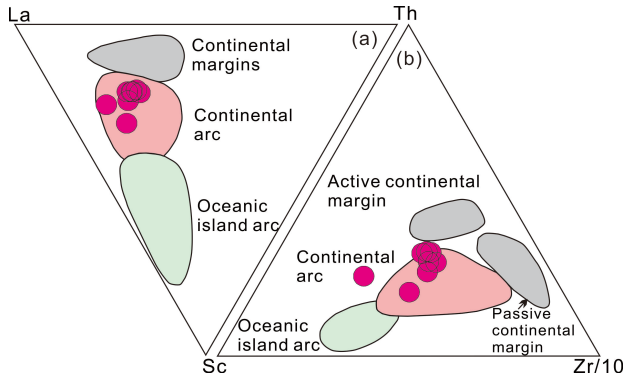


Figure 12: Tectonic setting discrimination diagrams for clastic rocks from the Linxi Formation. (a) La–Th–Sc diagram; (b) Th–Zr/10–Sc diagram (after Bhatia and Crook [107]).

The characteristics of REEs are often used to determine the tectonic setting and/or provenance of modern and ancient sediments. Murry [109] showed that the sign and size of Ce anomalies can be used to help distinguish the tectonic setting of sedimentary basins. Taking the content of REEs in North American shale as the reference value, spreading ridges within 400km from the top of the ridge are characterized by pronounced negative Ce anomalies, with a Ce content of 0.29; ocean basins show a moderate negative Ce anomaly of 0.55, and continental margins have negligible or slight positive Ce anomalies of 0.9–1.30. The studied clastic rocks display weak negative Ce anomalies, ranging from 0.87 to 0.96, suggesting that the sedimentary environment during the deposition of the Linxi Formation was located close to a continental margin.

The Mg:Al ratios of sedimentary rocks [b = 100 × ($MgO/Al_2O_3$)] can be used to infer the salinity of water masses [110]. Freshwater sedimentary settings have b values of <1, land–sea transitional settings have b values of 1–10, seawater has b values of 10–500, and epicontinental sea settings (or lagoon carbonate sedimentary environments) have b values of >500. Most measured b values for sedimentary rocks of the Linxi Formation range from 1 to 10 (6.9, 8.3), and a few range from 10 to 500, indicating these rocks were deposited in a transitional sedimentary environment. Zhang et al. [48] analyzed the palaeosalinity in the study area and proposed a gradual desalination during the period of deposition of the Linxi Formation, from brackish water during deposition of the lower part

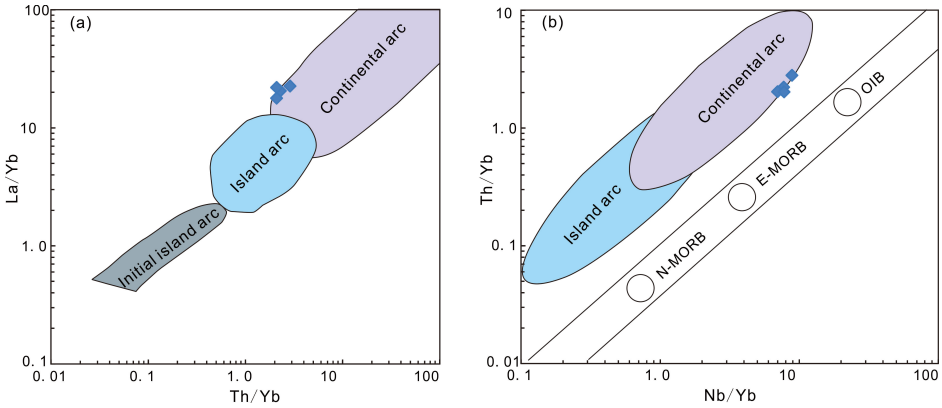


FIGURE 13: Tectonic discrimination diagrams for andesitic tuff samples from the Linxi Formation. (a) La/Yb versus Th/Yb diagram (after Condie [121]); (b) Th/Yb versus Nb/Yb diagram (after Pearce and Peate [122]). E-MORB – enriched mid-oceanridge basalt; N-MORB – normal MORB; OIB – ocean island basalt.

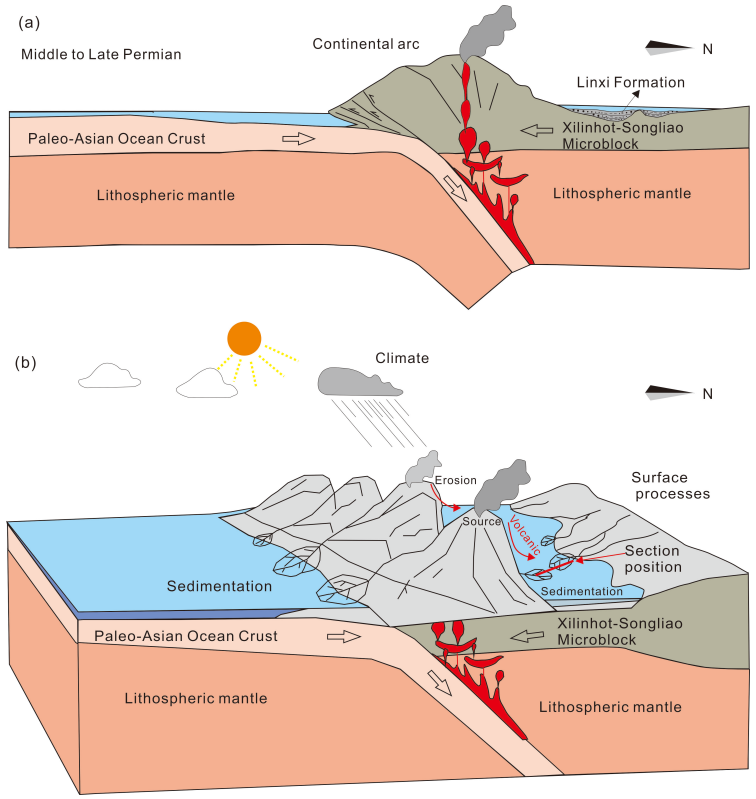


FIGURE 14: Schematic diagrams showing (a) the formation of the Linxi Formation and (b) the provenance of the clastic rocks in the formation.

to a freshwater lake setting during deposition of the upper part. Li et al. [111] considered that the Linxi Formation was formed in a continental sedimentary setting, with marine–continental interaction during the early stage of its deposition. Zhang et al. [112] identified marine fossils in the upper part of the Linxi Formation in the study area, from which they inferred both marine and continental sedimentary environments during the deposition of the Linxi Formation. These inferred sedimentary settings indicate that the PAO was not completely closed during the late Guadalupian.

In summary, strata of the Linxi Formation were deposited during the late Guadalupian in or near a continental arc. During the period of deposition, the PAO plate continued to subduct northward beneath the northern Songliao–Xilinhot block (Figure 14), with partial melting of the lithospheric mantle generating magma that ascended to form a continental arc. The magmatic rocks of the arc were denuded, with the eroded products being deposited in a continental arc basin and forming the sediment supply for the Linxi Formation (Figure 14). Zhang et al. [113] considered that the Linxi Formation

was deposited in a continental arc during the closure of the PAO, with a transition from subduction to collision during the late Permian. With continuing subduction, collision, and associated uplift of continental crust during the latest Guadalupian, the depositional setting of the Linxi Formation gradually changed from a marine–continental transitional setting to a continental environment, with the water gradually changing from brackish to fresh. The final closure of the PAO occurred after 262.2 ± 1.1 Ma, which is the age of the Linxi Formation tuff dated in this study.

## 6. Conclusions

Our petrological, geochemical, and isotope geochronological study of the Permian Linxi Formation in Northeast China allows the following conclusions to be drawn.

(1) Zircon U–Pb dating of an andesitic tuff from the Taohaiyingzi section of the Linxi Formation yielded an age of 262.2 ± 1.1 Ma, which is the first precise age reported for volcanic rocks from the formation. Combining this new date with existing palaeontological and detrital zircon age data, deposition of the Linxi Formation is inferred to have occurred from the late Guadalupian to the Lopingian.

(2) Geochemical characteristics of clastic rocks of the Linxi Formation show that they are of low maturity and were deposited near the source. Provenance weathering indicators reveal that the sediments were derived from source rocks in a continental arc setting and were not recycled. In addition, the source area was characterized by weak–moderate chemical weathering under a warm and humid climate.

(3) The PAO plate was subducted northward in Northeast China. The source rocks of the Linxi Formation were mainly immature felsic magmatic rocks that formed in a continental arc generated by the subduction of Paleo-Asian oceanic crust beneath the Xilinhot–Songliao block. The Linxi Formation was deposited in a back-arc basin setting adjacent to a continental arc. Deposition of the Linxi Formation overlapped with the transition from subduction to PAO closure, which occurred after 262.2 ± 1.1 Ma.

## Data Availability

The data used in this study are available in the Supplementary Material.

## Conflicts of Interest

The authors declare that they have no conflicts of interest.

## Acknowledgments

The authors thank Professor Simon A. Wilde for his careful revision and constructive comments on an earlier version of this paper. This study was supported by funding from the National Key R&D Program of China (2019YFC0605404 and 41790451), China Geological Survey Projects (DD20221664 and DD20230210), the Invertigation on the Middle Jurassic Flora and Strata in the Central and Southern Great Xing`an Range, NE China (42172024), the National Natural Science Foundation of China (NSFC 42293280), the Strategic Priority Research Programs of the Chinese Academy of Sciences (XDB26000000), and CAS (QYZDY-SSW-DQC023). We thank Professor Wenchun Ge for conducting the isotope analyses. We appreciate constructive comments from the editor and reviewers regarding an earlier version of this paper.

## Supplementary Materials

Supplementary Table S1: U–Pb isotope composition of andesitic tuff from the Linxi Formation.
Supplementary Table S2: Major and trace element compositions of clastic rocks from the Linxi Formation (wt% for major oxides; ppm for trace elements).

## References

[1] A. M. C. Şengör, B. A. Natal'in, and V. S. Burtman, "Evolution of the Altaid Tectonic collage and Palaeozoic Crustal growth in Eurasia," *Nature*, vol. 364, no. 6435, pp. 299–307, 1993.

[2] A. M. C. Şengör, B. A. Natal'in, G. Sunal, and R. van der Voo, "The Tectonics of the Altaids: Crustal growth during the construction of the Continental Lithosphere of central Asia between 750 and 130 ma ago," *Annual Review of Earth and Planetary Sciences*, vol. 46, no. 1, pp. 439–494, 2018. https://www.annualreviews.org/toc/earth/46/1.

[3] B. F. Windley, A. Kröner, J. Guo, G. Qu, Y. Li, and C. Zhang, "Neoproterozoic to Paleozoic geology of the Altai Orogen, NW China: new Zircon age data and Tectonic evolution, " *The Journal of Geology*, vol. 110, no. 6, pp. 719–737, 2002.

[4] B. F. Windley, D. Alexeiev, W. Xiao, A. Kröner, and G. Badarch, "Tectonic models for accretion of the central Asian Orogenic belt," *Journal of the Geological Society*, vol. 164, no. 1, pp. 31–47, 2007.

[5] W. Xiao, B. F. Windley, J. Hao, and M. Zhai, "Accretion leading to collision and the Permian Solonker Suture, inner Mongolia, China: Termination of the central Asian Orogenic belt," *Tectonics*, vol. 22, no. 6, 2003.

[6] W. Xiao, B. F. Windley, S. Sun, et al., "A tale of amalgamation of three Permo-Triassic collage systems in central Asia: Oroclines, Sutures, and terminal accretion," *Annual Review of Earth and Planetary Sciences*, vol. 43, no. 1, pp. 477–507, 2015. https://www.annualreviews.org/toc/earth/43/1.

[7] G.-Y. Li, L. Qiu, Z.-D. Li, et al., "Closure of the Eastern paleo-Asian ocean: Constraints from the age and geochemistry of early Permian Zhaojinggou Pluton in inner

Mongolia (North China)," *Minerals*, vol. 12, no. 6, p. 738, 2022.

[8] H. D. Li, J. B. Zhou, and S. A. Wilde, "Nature and development of the South Tianshan-Solonker Suture zone," *Earth-Science Reviews*, vol. 233, October, p. 104189, 2022.

[9] Q. Ren, S. Zhang, M. Hou, et al., "New early Permian Paleomagnetic and Geochronological data from the Xilinhot-Songliao block and their implications for the relationship between the paleo-Asian ocean and the paleo-Tethys ocean," *Geophysical Research Letters*, vol. 49, no. 19, 2022.

[10] D. H. Zhang, G. C. Zhao, B. C. Huang, J. Zhao, and Q. Zhao, "Palaeomagnetic constraints on a late Permian to early Triassic final closure of the Palaeo-Asian ocean," *Geological Journal*, vol. 58, no. 2, pp. 903–919, 2023. https://onlinelibrary.wiley.com/toc/10991034/58/2.

[11] W. J. Xiao, B. F. Windley, B. C. Huang, et al., "End-Permian to mid-Triassic termination of the Accretionary processes of the Southern Altaids: Implications for the Geodynamic evolution, Phanerozoic Continental growth, and Metallogeny of central Asia," *International Journal of Earth Sciences*, vol. 98, no. 6, pp. 1189–1217, 2009.

[12] W. J. Xiao, B. F. Windley, C. Yuan, et al., "Paleozoic multiple Subduction-accretion processes of the Southern Altaids," *American Journal of Science*, vol. 309, no. 3, pp. 221–270, 2009.

[13] W. Xiao, B. F. Windley, C. Han, et al., "Late Paleozoic to early Triassic multiple roll-back and Oroclinal bending of the Mongolia collage in central Asia," *Earth-Science Reviews*, vol. 186, November, pp. 94–128, 2018.

[14] J.-B. Zhou and S. A. Wilde, "The Crustal accretion history and Tectonic evolution of the NE China segment of the central Asian Orogenic belt," *Gondwana Research*, vol. 23, no. 4, pp. 1365–1377, 2013.

[15] J. B. Zhou, S. A. Wilde, G. C. Zhao, and J. Han, "Nature and assembly of Microcontinental blocks within the paleo-Asian ocean," *Earth-Science Reviews*, vol. 186, November, pp. 76–93, 2018.

[16] Y. J. Liu, W. M. Li, Z. Q. Feng, Q. B. Wen, F. Neubauer, and C. Y. Liang, "A review of the Paleozoic Tectonics in the Eastern part of central Asian Orogenic belt," *Gondwana Research*, vol. 43, March, pp. 123–148, 2017.

[17] C. W. Wang, W. Jin, X. Z. Zhang, Z. H. Ma, and N. Li, "New understanding of the late Paleozonic Tectonics in northeastern China and adjacent areas," *Journal of Stratigraphy*, vol. 32, no. 2, pp. 119–136, 2008.

[18] F. Wu, D. Sun, H. Li, B. Jahn, and S. Wilde, "A-type Granites in northeastern China: Age and Geochemical constraints on their Petrogenesis," *Chemical Geology*, vol. 187, nos. 1–2, pp. 143–173, 2002.

[19] F. Wu, S. A. Wilde, G. Zhang, and D. Sun, "Geochronology and Petrogenesis of the post-Orogenic cu–NI sulfide-bearing Mafic–Ultramafic complexes in Jilin province, NE China," *Journal of Asian Earth Sciences*, vol. 23, no. 5, pp. 781–797, 2004.

[20] Q. Shang, "Occurrences of Permian RA-Diolarians in central and East-Ern Nei Mongol (inner mon-Golia) and their geological Sig-Nificance to the northern China Orogen," *Chinese Science Bulletin*, vol. 49, no. 24, p. 2613, 2004.

[21] D. Y. Sun, F. Y. Wu, Y. B. Zhang, and S. Gao, "The final closing time of the West Lamulun river-Changchun-Yanji plate Suture zone-evidence from the Dayushan Granitic Pluton, Jilin province," *Journal of Jilin University: Earth Science Edition*, vol. 34, no. 2, pp. 174–178, 2004.

[22] Y. B. Zhang, F. Y. Wu, M. G. Qu, and X. P. Lu, "The Tectonic attribute of the Helong block and Eastern boundary on the Eastern margin of the North China platform," *Science in China (Series D: Earth Sciences)*, vol. 34, no. 9, pp. 795–806, 2004.

[23] J. Y. Li, L. M. Gao, G. H. Sun, Y. P. Li, and Y. B. Wang, "Shuangjingzi middle Triassic Syn-Collisional crust derived granite in the east inner Mongolia and its constraint on the timing of collision between Siberian and Sino Korean paleo-plates," *Acta Petrologica Sinica*, vol. 23, no. 3, pp. 565–582, 2007.

[24] C. Z. Cao, F. l. Yang, C. Tian, and C. Yuan, "The Ophiolite and the position of Suture belt from Sino–Korean plate and Siberian plates in Hegenshan area, inner Mongolia," in *The Symposium of plate tectonics in Northern China*, pp. 64–86, Geological Publishing Press, Beijing, 1986.

[25] B. Xu and B. Chen, "The structure and evolution of Mesozoic-Paleozoic Orogenic belt between the Huabei plate and Siberia plate in the northern inner Mongolia," *Science in China (Series D)*, vol. 27, no. 3, pp. 227–232, 1997.

[26] P. T. Robinson, M. Zhou, X.-F. Hu, P. Reynolds, B. Wenji, and J. Yang, "Geochemical Constraintson the origin of the Hegenshan Ophiolite, inner Mongolia, China," *Journal of Asian Earth Sciences*, vol. 17, no. 4, pp. 423–442, 1999.

[27] T. Nozaka and Y. Liu, "Petrology of the Hegenshan Ophiolite and its implication for the Tectonic evolution of northern China," *Earth and Planetary Science Letters*, vol. 202, no. 1, pp. 89–104, 2002.

[28] K. D. Tang, "Tectonic development of Paleozoic Foldbelts at the North margin of the Sino-Korean Craton," *Tectonics*, vol. 9, no. 2, pp. 249–260, 1990.

[29] J. A. Shao, *The Crustal Evolution in Northern Margin Middle Segment of the Sino-Korean Plate*, Peking University Press, Beijing, 1991.

[30] H. Dawei, H. Huaizeng, X. Yïjun, X. Haiming, and J. Manyuan, "Permian alkaline Granites in central inner Mongolia and their Geodynamic Significance1," *Acta Geologica Sinica - English Edition*, vol. 8, no. 1, pp. 27–39, 1995 http://doi.wiley.com/10.1111/acgs.1995.8.issue-1.

[31] Y. L. Li, H. W. Zhou, Z. Q. Zhong, X. H. Zhang, Q. N. Liao, and M. C. Ge, "Collision processes of North China and Siberian plates: Evidence from LA-ICP-MS Zircon U-PB age on deformed granite in Xar Moron Suture zone," *Earth Science: Journal of China University of Geosciences*, vol. 34, no. 6, pp. 931–938, 2009.

[32] Y. L. Li, H. W. Zhou, W. J. Xiao, Z. Q. Zhong, S. P. Yin, and F. L. Li, "Superposition of paleo-Asian and West-Pacific Tectonic domains in the Eastern section of the Solonker Suture zone: Insight from Petrology, geochemistry and Geochronology of Deformde Diorite in Xar Moron fault zone, inner Mongolia," *Earth Science: Journal of China University of Geosciences*, vol. 37, no. 3, pp. 433–450, 2012.

[33] G. Q. Han, Y. J. Liu, Q. B. Wen, et al, "LA–ICP–MS U–PB dating of Detrital Zircons from the Permian Sandstones in

North side of Xar Moron river Suture belt and its Tectonic implications," *Earth Science-Journal of China University of Geosciences*, vol. 36, no. 4, pp. 687–702, 2011.

[34] X. S. Ye, Q. N. Liao, and M. C. Ge, "Petrogenesis and Tectonic significance of Triassic Peraluminous Granitoids in Xilinhaote and Linxi area, inner Mongolia," *Geological Science and Technology Information*, vol. 30, no. 3, pp. 57–64, 2011.

[35] Y. J. Zheng, J. Zhang, S. W. Chen, X. Huang, L. J. Zhang, and W. L. Wang, "New fossil discovery along the section of Linxi formation at Taohaiyingzi in Ar Horqin banner, inner Mongolia," *Geological Bulletin of China*, vol. 32, no. 8, pp. 1269–1276, 2013.

[36] Y. J. Zheng, H. H. Zhang, S. W. Chen, et al, "LA-ICP-MS U-PB age of Detrital Zircons from late Permian Linxi Formationin Ar Horqin banner, inner Mongolia," *Geological Bulletin of China*, vol. 33, no. 9, pp. 1293–1307, 2014.

[37] S. Z. Shen, H. Zhang, Q. H. Shang, and W. Z. Li, "Permian Stratigraphy and correlation of northeast China: A review," *Journal of Asian Earth Sciences*, vol. 26, nos. 3–4, pp. 304–326, 2006.

[38] P. R. Eizenhöfer and G. Zhao, "Solonker Suture in East Asia and its bearing on the final closure of the Eastern segment of the Palaeo-Asian ocean," *Earth-Science Reviews*, vol. 186, November, pp. 153–172, 2018.

[39] X. Wu, Y. Shi, and J. L. Anderson, "SHRIMP U-PB dating of Detrital Zircons from the Permian Sandstones along the Southern and northern margins of Xar Moron river, central inner Mongolia: implications for provenance and the Tectonic evolution of the Eastern segment of the central Asian Orogenic belt," *American Journal of Science*, vol. 321, nos. 1–2, pp. 152–177, 2021.

[40] B. H. Huang, "Plant fossils of the Taohaiyingzi formation in the Eastern inner Mongolia," *Plant Journal*, vol. 26, no. 6, pp. 580–583, 1983.

[41] Y. S. Zhang, S. W. Tian, S. G. Niu, et al, "The discovery of Conchostracan fossils in the upper Permian Linxi formation of Linxi area, inner Mongolia, and its geological significance," *Geological Bulletin of China*, vol. 31, no. 9, pp. 1394–1403, 2012.

[42] Z. J. He, S. W. Liu, and J. S. Ren, "Late Permian–early Triassic sedimentary evolution and Tectonic setting of the Linxi region, inner Mongolia," *Regional Geology of China*, vol. 16, no. 4, pp. 403–427, 1997.

[43] H. Z. Yu, "Sedimentary Facies and Palaeogeography of the Songliao basin and its peripheral areas during Carboniferous-Permian time," *Sedimentary Geology and Tethyan Geology*, vol. 21, no. 4, pp. 70–83, 2001.

[44] P. R. Eizenhöfer, G. Zhao, J. Zhang, and M. Sun, "Final closure of the Paleo-Asian ocean along the Solonker Suture zone: Constraints from Geochronological and Geochemical data of Permian volcanic and sedimentary rocks," *Tectonics*, vol. 33, no. 4, pp. 441–463, 2014.

[45] Y. Z. Wang, G. J. Qin, and Q. OU., "A study on the upper-Permian Linxi formation on the Dajing copper-tin Polymetallic mine, Linxi, inner Mongolia," *Mineral Resources and Geology*, vol. 15, no. 83, pp. 205–211, 2001.

[46] R. K. Zhu, H. X. Xu, S. H. Deng, and H. L. Guo, "Lithofacies Palaeogeography of the Permian in northern China," *Journal of Palaeogeography*, vol. 9, no. 2, pp. 133–142, 2007.

[47] S. W. Chen, Q. H. Ding, Y. J. Zheng, et al, "New areas and series of Strata on the periphery of Songliao Basin: The progress and recognition based on Foundational geological survey for oil and gas resources," *Geological Bulletin of China*, vol. 32, no. 8, pp. 1147–1158, 2013.

[48] J. Zhang, X. H. Li, Y. J. Zheng, F. Su, and Z. Zhen, "Analysis on the Pleosalinity of upper Permian Linxi formation in Jaruo area, inner Mongolia," *Geology and Resources*, vol. 22, no. 6, pp. 471–477, 2013.

[49] H. Zhang, C. Cao, X. Liu, et al., "The terrestrial end-Permian mass extinction in South China," *Palaeogeography, Palaeoclimatology, Palaeoecology*, vol. 448, April, pp. 108–124, 2016.

[50] H. Zhang and S. Shen, "What caused the five mass Extinctions (in Chinese)," *Chinese Science Bulletin*, vol. 62, no. 11, pp. 1119–1135, 2017.

[51] S. Z. Shen and J. Y. Rong, "Preface: New advances in the integrative Stratigraphy and timescale of China," *Science China Earth Sciences*, vol. 62, no. 1, pp. 1–6, 2019.

[52] S. Shen, H. Zhang, Y. Zhang, et al., "Permian integrative Stratigraphy and timescale of China," *Science China Earth Sciences*, vol. 62, no. 1, pp. 154–188, 2019.

[53] L. Xiang, H. Zhang, S. D. Schoepfer, et al., "Oceanic redox evolution around the end-Permian mass extinction at Meishan, South China," *Palaeogeography, Palaeoclimatology, Palaeoecology*, vol. 544, April, p. 109626, 2020.

[54] Q. Wu, J. Ramezani, H. Zhang, et al., "High-precision U-PB age constraints on the Permian floral turnovers, Paleoclimate change and Tectonics of North China," *Geology*, vol. 49, no. 6, pp. 677–681, 2021.

[55] Y. J. Zheng, F. Su, S. N. Chang, J. Zhang, X. Huang, and S. W. Chen, "New understanding of the upper Permian Linxi formation in Southern Daxinganling region," *Geology and Resources*, vol. 23, no. 1, pp. 25–30, 2014.

[56] H. H. Zhang, Y. J. Zheng, S. W. Chen, et al, "LA-ICP-MS U-PB Geochronology of Detrital Zircons from Permian in Baarin left banner of inner Mogolia and its Tectonic significance," *Acta Geologica Sinica*, vol. 89, no. 10, pp. 1703–1717, 2015.

[57] D. D. Wang, S. Z. Li, X. G. Zhou, et al, "SHRIMP U-PB dating of Detrital Zircon from the upper Permian Linxi formation in Eastern inner Mongolia, and its geological significance," *Geological Review*, vol. 62, no. 4, pp. 1021–1040, 2016.

[58] X. H. Zhang, H. F. Zhang, Y. J. Tang, S. A. Wilde, and Z. C. Hu, "Geochemistry of Permian Bimodal volcanic rocks from central inner Mongolia North China implication for Tectonic setting and Phanerozoic Continental growth in central Asian Orogenic belt," *Chemical Geology*, vol. 249, nos. 3–4, pp. 262–281, 2008.

[59] Y.-F. Ma, Y.-J. Liu, Y. Wang, et al., "Geochronology, Petrogenesis, and Tectonic implications of Permian Felsic rocks of the central great Xing'An range, NE China," *International Journal of Earth Sciences*, vol. 108, no. 2, pp. 427–453, 2019.

[60] W. L. Wang, "Late Permian Conchostraca from the Taohaiyingzi formation in Ju Ud Meng, Nei Mongolia," *Acta Palaeontologica Sinica*, vol. 23, no. 1, pp. 124–131, 1984.

[61] N. J. G. Pearce, W. T. Perkins, J. A. Westgate, et al., "A compilation of new and published major and trace element data for NIST SRM 610 and NIST SRM 612 glass reference materials," *Geostandards and Geoanalytical Research*, vol. 21, no. 1, pp. 115–144, 1997. http://doi.wiley.com/10.1111/ggr.1997.21.issue-1.

[62] L. P. Black, S. L. Kamo, C. M. Allen, et al., "TEMORA 1: A new Zircon standard for Phanerozoic U-PB Geochronology," *Chemical Geology*, vol. 200, nos. 1–2, pp. 155–170, 2003.

[63] X. H. Li, G. Q. Tang, B. Guo, et al, "Qinghu Zircon: A working reference for Microbeam analysis of U-PB age and HF and O Isotopes," *Chinese Science Bulletin*, vol. 58, no. 20, pp. 1954–1961, 2013.

[64] S. E. Jackson, N. J. Pearson, W. L. Griffin, and E. A. Belousova, "The application of Laserablation-Inductively coupled plasma-mass Spectrometry to in situ U–PB Zircon Geochronology," *Chemical Geology*, vol. 211, nos. 1–2, pp. 47–69, 2004.

[65] T. Andersen, "Correction of common lead in U-PB analyses that do not report $^{204}$PB," *Chemical Geology*, vol. 192, nos. 1–2, pp. 59–79, 2002.

[66] M. Wiedenbeck, P. Allé, F. Corfu, et al., "Three natural Zircon standards for U-th-PB, LU-HF, trace element and REE analyses," *Geostandards and Geoanalytical Research*, vol. 19, no. 1, pp. 1–23, 1995. http://doi.wiley.com/10.1111/ggr.1995.19.issue-1.

[67] K. R. Ludwig, *User's Manual for Isoplot 3.0. A Geochronological Toolkit for Microsoft Excel,* Berkeley Geochronology Center, 2003.

[68] Q. Liang, "Determination of trace elements in Granites by Inductively coupled plasma mass Spectrometry," *Talanta*, vol. 51, no. 3, pp. 507–513, 2000.

[69] X. X. Gu, J. M. Liu, M. H. Zheng, J. X. Tang, and L. Qi, "Provenance and Tectonic setting of the Proterozoic Turbidites in Hunan, South China: Geochemical evidence," *Journal of Sedimentary Research*, vol. 72, no. 3, pp. 393–407, 2002.

[70] R. Cox, D. R. Lowe, and R. L. Cullers, "The influence of sediment recycling and basement composition on evolution of Mudrock chemistry in the Southwestern United States," *Geochimica et Cosmochimica Acta*, vol. 59, no. 14, pp. 2919–2940, 1995.

[71] S. R. Taylor, and S. M. McLennan, "The continental crust: its composition and evolution", Oxford: Blackwell Scientific, pp. 312, 1985.

[72] S. M. McLennan, S. R. Taylor, M. T. McCulloch, and J. B. Maynard, "Geochemical and Nd Sr isotopic composition of deep-sea Turbidites: Crustal evolution and plate Tectonic associations," *Geochimica et Cosmochimica Acta*, vol. 54, no. 7, pp. 2015–2050, 1990.

[73] H. H. Zhang, Y. J. Zheng, J. Zhang, et al, "LA - ICP - MS Zircon U-PB age and its Tectonic significance of Clastic rocks from late Permian Linxi formation in Aluke'Erqin Qi, inner Mogolia," *Geological Journal of China Universities*, vol. 25, no. 1, pp. 14–23, 2019.

[74] J. Han, J. B. Zhou, X. Z. Zhang, and H. J. Qiu, "Detrital Zircon U-PB dating from Sandstone of the upper Permian Linxi formation, Linxi area, inner Mongolia, China and its Tectonic implications," *Geological Bulletin of China*, vol. 30, no. 2~3, pp. 258–269, 2011.

[75] W. W. Song, J. B. Zhou, X. D. Guo, and Y. K. Li, "Geotectonic setting of Songliao block: Reatriction from Paleozoic Detrital Zircon U-PB dating," *Global Geology*, vol. 31, no. 3, pp. 522–535, 2012.

[76] S. W. Chen, H. H. Zhang, Y. J. Zheng, et al, "Determination of Linxi formation and geological significance in the late Permian, in Keerqinyouyizhongqi inner Mongolia: From the evidence of Detrital Zircon LA-ICP-MS U-PB chronology," *Geological Bulletin of China*, vol. 34, no. 10, pp. 1869–1877, 2015.

[77] B. P. Roser and R. J. Korsch, "Geochemical characterization,evolution and source of a Mesozoic Accretionary wedge: The Torlesse Terrane, New Zealand," *Geological Magazine*, vol. 136, no. 5, pp. 493–512, 1999.

[78] R. L. Cullers, "The controls on the major and trace-element evolution of Shales, Siltstones and Sandstones of Ordovician to tertiary age in the wet mountain region," *Chemical Geology*, vol. 123, nos. 1–4, pp. 107–131, 1995.

[79] L. E. Savoy, R. K. Stevenson, and E. W. Mountjoy, "Provenance of upper Devonnian-lower Carboniferous Miogeoclinal STATA, southeastern Canadian Cordillera: Link between Tectonics and sedimentation," *Journal of Sedimentary Research*, vol. 70, no. 1, pp. 181–193, 2000.

[80] S. L. Liu, Y. H. Liu, G. Lin, Y. Zhou, F. X. Gong, and D. S. Zhang, "REE Geochemical characteristics and geological significance of Mudstones from Neogene, Nanpu sag, Bohai Basin," *Geoscience*, vol. 20, no. 3, pp. 449–456, 2006.

[81] W. Z. Shen, L. S. Shu, L. Xiang, F. R. Zhang, and B. Wang, "Geochemical characteristics of early Paleozoic sedimentary rocks in the Jinggangshan area, Jianxi province and the constraining to the sedimentary Environmnet," *Acta Petrologica Sinica*, vol. 25, no. 10, pp. 2442–2458, 2009.

[82] Y. L. Zhang, Z. Q. Wang, Z. Yan, and T. Wang, "Tectonic setting of Neoproterozoic Beiyixi formation in Quruqtagh area, Xinjiang: Evidence from geochemistry of Clastic rocks," *Acta Petrologica Sinica*, vol. 27, no. 6, pp. 1785–1796, 2011.

[83] Q. Luo, N. Zhong, L. Zhu, et al., "Correlation of burial organic carbon and Paleoproductivity in the Mesoproterozoic Hongshuizhuang formation, northern North China," *Chinese Science Bulletin*, vol. 58, no. 11, pp. 1299–1309, 2013.

[84] J. W. Cui, Y. Y. Zheng, X. Sun, L. M. Tian, and J. Y. Sun, "Petrogenesis and Geodynamics characteristics of Ganglong in Thenorth of Songpan-Ganzi fold belt," *Geological Science and Technology Information*, vol. 35, no. 2, pp. 129–139, 2016.

[85] Q. Zhang, Y. F. Xiao, X. F. Wang, et al, "Geochemistry of the Longmaxi formation Mudstones of the Southwest Sichuan Basin: Implications for provenance and source weathering," *Geological Review*, vol. 66, no. 5, pp. 1393–1411, 2020.

[86] C. M. Fedo, H. Wayne Nesbitt, and G. M. Young, "Unraveling the effects of potassium Metasomatism in sedimentary rocks and Paleosols, with implications for Paleoweathering conditions and provenance," *Geology*, vol. 23, no. 10, p. 921, 1995.

[87] S. Sensarma, V. Rajamani, and J. K. Tripathi, "Petrography and Geochemical characteristics of the sediments of the small river Hemavati, southern India: Implications for provenance and weathering processes," *Sedimentary Geology*, vol. 205, nos. 3–4, pp. 111–125, 2008.

[88] C. L. Mou, X. Y. Ge, Q. Yu, et al, "Palaeoclimatology and provenance of black Shales from Wufeng–Longmaxi formations in southwestern Sichuan province: From Geochemical records of well Xindi-2," *Journal of Palaeogeography*, vol. 21, no. 5, pp. 835–846, 2019.

[89] H. W. Nesbitt, and G. M. Young, "Early Proterozoic climates and plate motions inferred from major element chemistry of lutites", Nature, vol. 299, no.5885, pp. 715–717, 1982.

[90] H. W. Nesbitt, and G. M. Young, "Prediction of some weathering trends of plutonic and volcanic rocks based on thermodynamic and kinetic considerations", Geochimica et Cosmochimica Acta, vol. 48, no.7, pp. 1523–1534, 1984.

[91] H. W. Nesbitt and G. M. Young, "Formation and Diagenesis of weathering profiles," *The Journal of Geology*, vol. 97, no. 2, pp. 129–147, 1989.

[92] R. L. Cullers and V. N. Podkovyrov, "Geochemistry of the Mesoproterozoic Lakhanda Shales in southeastern Yakutia, Russia: Implications for mineralogical and provenance control, and recycling," *Precambrian Research*, vol. 104, nos. 1–2, pp. 77–93, 2000.

[93] R. L. Cullers and V. N. Podkovyrov, "The source and origin of Terrigenous sedimentary rocks in the Mesoproterozoic Ui group,southeastern Russia," *Precambrian Research*, vol. 117, nos. 3–4, pp. 157–183, 2002.

[94] X. Long, M. Sun, C. Yuan, W. Xiao, and K. Cai, "Early Paleozoic sedimentary record of the Chinese Altai: Implications for its Tectonic evolution," *Sedimentary Geology*, vol. 208, nos. 3–4, pp. 88–100, 2008.

[95] P. C. van de Kamp and B. E. Leake, "Petrography and geochemistry of Feldspathic and Mafic sediments of the Northeastern Pacific margin, transact," *Transactions of the Royal Society of Edinburgh*, vol. 76, no. 4, pp. 411–449, 1985.

[96] X. T. Xu and L. Y. Shao, "Limiting factors in utilization of chemical index of alteration of Mudstones to quantify the degree of weathering in provenance," *Journal of Palaeogeography*, vol. 20, no. 3, pp. 515–522, 2018.

[97] X.-T. Xu, L.-Y. Shao, B. Lan, et al., "Continental chemical weathering during the early Cretaceous Oceanic Anoxic event (Oae1B): A case study from the Fuxin Fluvio-Lacustrine Basin, Liaoning province, NE China," *Journal of Palaeogeography*, vol. 9, no. 1, 2020.

[98] S. P. Verma, M. A. Rivera-Gómez, L. Díaz-González, et al., "Multidimensional classification of Magma types for altered igneous rocks and application to their Tectonomagmatic discrimination and igneous provenance of Siliciclastic sediments," *Lithos*, vols. 278–281, May, pp. 321–330, 2017.

[99] P. A. Floyd, J. A. Winchester, and R. G. Park, "Geochemistry and Tectonic setting of Lewisian Clastic Metasediments from the early Proterozoic Loch Maree group of Gairloch, NW Scotland," *Precambrian Research*, vol. 45, nos. 1–3, pp. 203–214, 1989.

[100] K. I. Hayashi, H. Fujisawa, H. D. Holland, and H. Ohmoto, "Geochemistry of approximately 1.9 Ga sedimentary rocks from northeastern Labrador, Canada," *Geochimica et Cosmochimica Acta*, vol. 61, no. 19, pp. 4115–4137, 1997.

[101] A. Vosoughi Moradi, A. Sarı, and P. Akkaya, "Geochemistry of the Miocene oil shale (Hanili formation) in the Ankr-Orum Basin, central Turkey: Implications for Paleoclimate conditions, source-area weathering, provenance and Tectonic setting," *Sedimentary Geology*, vol. 341, July, pp. 289–303, 2016.

[102] R. L. Rudnick, S. Gao, W. Ling, Y. Liu, and W. F. McDonough, "Petrology and geochemistry of Spinel Peridotite Xenoliths from Hannuoba and Qixia, North China Craton," *Lithos*, vol. 77, nos. 1–4, pp. 609–637, 2004.

[103] G. H. Girty, D. L. Ridge, and C. Knaack, "Provenance and Depositional setting of Paleozoic Chert and Argillite, Sierra Nevada, California," *SEPM Journal of Sedimentary Research*, vol. Vol. 66, no. 1, pp. 107–118, 1996.

[104] H. H. Zhang, J. Zhang, F. Su, et al, "Geochemical characteristics of Mudstone from the late Permian Linxi formation in Aluke'Erqin Qi, inner Mogolia and its structural significance," *Acta Geologica Sinica*, vol. 93, no. 5, pp. 1125–1136, 2019.

[105] Z. Zhen, S. W. Chen, Y. J. Zheng, et al, "Geochemical characteristics of Linxi formation along Taohaiyingzi section in Ar Horqin banner, inner Mongolia, and the constraint on the Provenances and the Tectonic settings," *Geology in China*, vol. 45, no. 5, pp. 1011–1022, 2018.

[106] X. H. Xiong and J. F. Xiao, "Geochemical indicators of sedimentary environments—A summary," *Earth and Environment*, vol. 39, no. 3, pp. 405–414, 2011.

[107] M. R. Bhatia and K. A. W. Crook, "Trace element characteristics of Graywackes and Tectonic setting discrimination of sedimentary basins," *Contributions to Mineralogy and Petrology*, vol. 92, no. 2, pp. 181–193, 1986.

[108] R. McCulloch and P. E. Rossi, "A Bayesian approach to testing the arbitrage pricing theory," *Journal of Econometrics*, vol. 49, nos. 1–2, pp. 141–168, 1991.

[109] R. W. Murray, M. R. Buchholtz ten Brink, D. L. Jones, D. C. Gerlach, and G. P. Russ III, "Rare earth elements as indicators of different marine Depositional environments in Chert and shale," *Geology*, vol. 18, no. 3, p. 268, 1990.

[110] K. M. Wang and S. S. Luo, "Geochemical characteristics and environmental significance of Gaoyuzhuang and Yangzhuang formations in Yanshan region," *Bulletin of Mineralogy, Petrology and Geochemistry*, vol. 28, no. 4, pp. 356–364, 2009.

[111] F. L. Li, X. Y. Qu, L. Liu, M. D. Yang, D. H. Wang, and G. X. Zhao, "Sedimentary environment on upper Permian Linxi group in inner Mongolia," *Acta Sedmentologica Sinica*, vol. 27, no. 2, pp. 265–272, 2009.

[112] Y. S. Zhang, S. G. Tian, and Z. X. Li, "Discovery of Marine fossils in the upper part of the Permaian Linxi formation in Lopingian, Xingmeng area, China" *Chinese Science Bulletin*, vol. 58, pp. 3429–3439, 2013.

[113] H. Zhang, L. Qiu, D.-P. Yan, et al., "Late-Permian Subduction-to-collision transition and closure of paleo-Asian ocean in Eastern central Asian Orogenic belt: Multidisciplinary evidence of Borehole cores from Songliao Basin, northeast China," *Gondwana Research*, vol. 122, October, pp. 74–92, 2023.

[114] S.-L. Sun, S.-W. Chen, Z.-J. Yang, et al., "Age of the Tuchengzi formation in Western Liaoning province and the Jurassic-Cretaceous boundary from the continuous core records of well Yd1," *Minerals*, vol. 12, no. 8, p. 953, 2022.

[115] R. W. L. Maitre, *A Classification of Igneous Rocks and Glossary of Terms*, Blackwell Scientific, Oxford, 1989.

[116] J. A. Winchester and P. A. Floyd, "Geochemical discrimination of different Magma series and their differentiation products using immobile elements," *Chemical Geology*, vol. 20, pp. 325–343, 1977.

[117] A. Peccerillo and S. R. Taylor, "Geochemistry of Eocene Calc-alkaline volcanic rocks from the Kastamonu area, northern Turkey," *Contributions to Mineralogy and Petrology*, vol. 58, no. 1, pp. 63–81, 1976.

[118] W. V. Boynton, "Cosmochemistry of the rare earth elements: Meteoritestudies," in *Rare Earth Element Geochemistry*, P. Henderson, Ed., pp. 63–114, Elsevier, Amsterdam, 1984.

[119] S. -S. Sun and W. F. McDonough, "Chemical and isotopic SYSTEMATICS of Oceanic Basalts: Implications for Mantle composition and processes," *Geological Society, London, Special Publications*, vol. 42, no. 1, pp. 313–345, 1989.

[120] P. A. Floyd, R. Shail, B. E. Leveridge, and W. Franke, "Geochemistry and provenance of Rhenohercynian Synorogenic Sandstone: Implications for Tectonic environment discrimination," *Geological Society, London, Special Publications*, vol. 57, no. 1, pp. 173–188, 1991.

[121] K. C. Condie, "Geochemical changes in Baslts and Andesites across the Archean-Proterozoic boundary: Identification and significance," *Lithos*, vol. 23, nos. 1–2, pp. 1–18, 1989.

[122] J. A. Pearce and D. W. Peate, "Tectonic implications of the composition of volcanic ARC Magmas," *Annual Review of Earth and Planetary Sciences*, vol. 23, no. 1, pp. 251–285, 1995. https://www.annualreviews.org/toc/earth/23/1.